

DOKUZ EYLÜL UNIVERSITY
GRADUATE SCHOOL OF NATURAL AND APPLIED SCIENCES

**NUMERICAL STUDY OF HEAT TRANSFER AND
FLOW CHARACTERISTICS OF THERMAL
SYSTEMS**

by
Utku Alp YÜCEKAYA

June, 2017
İZMİR

NUMERICAL STUDY OF HEAT TRANSFER AND FLOW CHARACTERISTICS OF THERMAL SYSTEMS

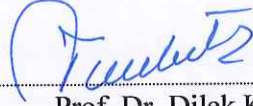
**A Thesis Submitted to the
Graduate School of Natural and Applied Sciences of Dokuz Eylül University
In Partial Fulfillment of the Requirements for the Master of Science of
Department of Mechanical Engineering**

**by
Utku Alp YÜCEKAYA**

**June, 2017
İZMİR**

M.Sc THESIS EXAMINATION RESULT FORM

We have read the thesis entitled "NUMERICAL STUDY OF HEAT TRANSFER AND FLOW CHARACTERISTICS OF THERMAL SYSTEMS" completed by UTKU ALP YÜCEKAYA under supervision of PROF. DR. DİLEK KUMLUTAŞ and we certify that in our opinion it is fully adequate, in scope and in quality, as a thesis for the degree of Master of Science.



Prof. Dr. Dilek Kumlutaş

Supervisor



Assoc. Prof. Dr. Can Özgür Çolpan

(Jury Member)



Asst. Prof. Dr. Hadli Garajehsarabi

(Jury Member)



Prof. Dr. Emine İlknur CÖCEN

Director

Graduate School of Natural and Applied Sciences

ACKNOWLEDGMENT

First of all, I would like to thank the project executive and my supervisor Prof. Dr. Dilek KUMLUTAŞ for providing every need and beyond for this thesis and our other studies. Without her determination, her hard work about this project and her guidance, this thesis cannot be accomplished.

I would like to specially thank to M. Sc. Özgün ÖZER for his advises, mental and scientific support and his help in experiments. I feel lucky and proud for working with him as a colleague and a student.

Also, I would like to express special thanks to my friends for their motivation and help.

I would like to express my sincere gratitude to my parents Mehmet YÜCEKAYA, Gülümay YÜCEKAYA, Burcu ÖZTÜRK and Ömer ÖZTÜRK for their endless encouragement, patience and valuable support in every part of my life.

Utku Alp YÜCEKAYA

NUMERICAL STUDY OF HEAT TRANSFER AND FLOW CHARACTERISTICS OF THERMAL SYSTEMS

ABSTRACT

The main purpose of air conditioning is to try to carry the health and comfort conditions that people have in their natural environment to indoors. These conditions related to parameters such as temperature, humidity and fresh air. However, these parameters can be examined in more detail by making use of current technological facilities. For example, in standards, there is only one value for comfort temperature of a room. However, the positions of the windows, doors, and other orifices that direct the conditioned air into the room create a volumetric inhomogeneous temperature distribution within the room. The flow characteristic of the conditioned air blown into the room, directly acts on this temperature distribution. Therefore, one of the two rooms with the average temperature (i.e. comfort temperature) may be quite comfortable and the other uncomfortable. In order to investigate this situation, the flow and heat transfer studies are very important in the room which includes conditioned air.

In the present study, using the Particle Image Velocimetry (PIV) method, three-dimensional velocity distribution of the outflow section of the indoor unit of the split air conditioner was obtained. In addition, the temperature distribution of the outflow section of the indoor unit of the split air conditioner was determined by the Meshed Infrared Temperature (MIT) measurement method. In addition, a three-dimensional version of the background-oriented Schlieren method was developed and the flow visualized according to the density difference.

The three-dimensional velocity and temperature distributions obtained by experimental methods are used as input in the numerical model created using the Computational Fluid Dynamics (CFD) method. Thus, the input conditions used in the CFD analyses were supported by experimental data, and the velocity and temperature distributions of the conditioned air in different boundary conditions were examined.

As a result of the study; velocity and temperature distributions were modeled close to the actual values of the conditioned air, and the effects of parameters such as velocity, temperature were investigated to each other and to the flow structure.

Keywords: Particle image velocimetry (PIV), computational fluid dynamics (CFD), split air conditioner, meshed infrared thermography (MIT), Schlieren method



ISIL SİSTEMLERİN ISI TRANSFERİ VE AKIŞ KARAKTERİSTİKLERİNİN SAYISAL İNCELENMESİ

ÖZ

İklimlendirmenin temel amacı, insanların doğal ortamlarında sahip oldukları sağlık ve konfor şartlarını iç mekâna taşımaya çalışmaktır. Bu şartlar temel anlamda bakıldığında; sıcaklık, nem, taze hava vb. parametreleri içerir. Ancak, güncel teknolojik imkânlardan faydalanarak bu parametreler daha detaylı incelenebilir. Örneğin; standartlarda, bir odanın konfor sıcaklığından bahsederken tek bir değer söz konusudur. Oysa odanın içinde bulunan pencere, kapı gibi unsurlar ve şartlandırılmış havayı içeriye yönlendiren menfezlerin konumu, oda içinde hacimsel homojen olmayan bir sıcaklık dağılımı oluşturmaktadır. Bu sıcaklık dağılımına, oda içerisine üflenen şartlandırılmış havanın akış karakteristiği, doğrudan etki etmektedir. Dolayısıyla, ortalama sıcaklığı konfor sıcaklığında olan iki odadan biri oldukça konforluyken diğeri konforsuz olabilir. Bu durumun araştırılabilmesi için iklimlendirilen hacimlerde akış ve ısı transferi incelemeleri oldukça önemlidir.

Mevcut çalışmada; Parçacık Görüntülemeli Hız Ölçümü (PGHÖ) yöntemi kullanarak split klima iç ünitesi çıkış ağzındaki hız dağılımı üç boyutlu olarak elde edilmiştir. Ayrıca, Ağ Yapılı Kızılötesi Sıcaklık Ölçümü (AYKSÖ) yöntemi ile split klima çıkış ağzının sıcaklık dağılımı belirlenmiştir. Ek olarak, arka plan konumlandırılmış Schlieren yönteminin üç boyutlu versiyonu geliştirilmiş ve yoğunluk farkına bağlı olarak akış görselleştirilmiştir.

DeneySEL yöntemler ile elde edilen üç boyutlu hız ve sıcaklık dağılımları Hesaplamalı Akışkanlar Dinamiği (HAD) yöntemi kullanarak oluşturulan sayısal modelde girdi olarak kullanılmıştır. Böylece, HAD analizlerinde kullanılan giriş koşulları deneySEL veriler ile desteklenerek, şartlandırılmış havanın farklı sınır şartları tanımlamalarında hız ve sıcaklık dağılımları incelenmiştir.

Yapılan çalışma sonucunda; iklimlendirilen hacimlerde hız ve sıcaklık dağılımlarının gerçeğe yakın modellenmesi sağlanmış olup, farklı sınır şartları için hız, sıcaklık gibi parametrelerin birbirlerine ve akış yapısına etkileri araştırılmıştır.

Anahtar Kelimeler: Parçacık görüntülemeli hız ölçümü (PGHÖ), hesaplamalı akışkanlar dinamiği (HAD), split klima, ağ yapılı kızılötesi sıcaklık ölçümü (AYKSÖ), Schlieren yöntemi



CONTENTS

	Page
M.Sc THESIS EXAMINATION RESULT FORM	ii
ACKNOWLEDGMENTS	iii
ABSTRACT	iv
ÖZ	vi
LIST OF FIGURES	x
LIST OF TABLES	xii
CHAPTER ONE - INTRODUCTION	1
1.1 Introduction	1
1.2 Literature Survey	1
1.3 Objective.....	4
CHAPTER TWO - EXPERIMENTAL STUDY.....	6
2.1 Particle Image Velocimetry (PIV).....	6
2.1.1 History of PIV	6
2.1.2 Methodology of PIV	9
2.1.3 Components of PIV	10
2.1.3.1 Seeding Particles.	11
2.1.3.2 Camera and Lenses.	12
2.1.3.3 Laser and Optics.....	13
2.1.3.4 Synchronizer.	14
2.1.4 PIV Setup Used in Current Study	14
2.2 Meshed Infrared Thermography (MIT).....	16
2.2.1 Infrared Thermography.....	17
2.2.2 Emissivity	18
2.2.3 Two Dimensional Meshed Infrared Thermography	19
2.2.4 Validation Experiment of Meshed Infrared Thermography	21

2.3 Alternative Flow Visualization Method: Three-Dimensional Background Oriented Schlieren Method (3DBOS)	24
2.4 Results of Experimental Study	28
CHAPTER THREE - NUMERICAL STUDY	33
3.1 Computational Fluid Dynamics (CFD)	33
3.1.1 History of CFD	33
3.1.2 The Mathematics of CFD	33
3.1.3 Conservation Laws	34
3.1.3.1 The Continuity Equation	34
3.1.3.2 The Momentum Equation	35
3.1.3.3 The Energy Equation	37
3.2 Numerical Study	39
3.2.1 CFD Model	40
3.2.2 Meshing	41
3.2.3 Boundary Conditions	46
3.2.4 Solver	48
CHAPTER FOUR - RESULTS AND DISSCUSSIONS	52
CHAPTER FIVE - CONCLUSION	61
REFERENCES	63

LIST OF FIGURES

	Page
Figure 2.1 Leonardo da Vinci's "a free water jet issuing from a square hole into a pool"	6
Figure 2.2 a) Leonardo da Vinci's aortic valve vortices, b) Velocity vectors from MRI in the left ventricular outflow tract.....	7
Figure 2.3 Ludwig Prandtl in front of his water tunnel for flow visualization	7
Figure 2.4 Separated flow behind wing, visualized with modern equipment in a replica of Ludwig Prandtl's tunnel.....	8
Figure 2.5 Vector map of instantaneous velocity field	9
Figure 2.6 Different particle distribution densities	12
Figure 2.7 The focal length and angle of view (AOV)	13
Figure 2.8 The schematic of SPIV setup.....	15
Figure 2.9 Photography of the SPIV setup.....	15
Figure 2.10 The calibration target with both cameras.....	16
Figure 2.11 The schematic of the MIT experiments	20
Figure 2.12 Velocity distribution for jet flow and measurement screens	21
Figure 2.13 The image of the validation experiments.....	22
Figure 2.14 The position of thermocouples	22
Figure 2.15 Steady state temperature measurements by PIIT (IR) and thermocouples (TC) at different points on the measurement mesh.....	23
Figure 2.16 Schematic representation of the BOS method.....	25
Figure 2.17 The result of the hot jet flow by BOS method.....	26
Figure 2.18 The experimental setup of 3DBOS method.....	27
Figure 2.19 PIV image at $z=165$ mm	29
Figure 2.20 The three-component volumetric average flow structure obtained by the PIV method	29
Figure 2.21 a) The result of the background-oriented Schlieren method obtained from the camera-1, b) The result of the background-oriented Schlieren method obtained from the camera-2, c) The result of the background-oriented Schlieren method obtained from the camera-3	30
Figure 2.22 The result of 3DBOS method	31

Figure 2.23 a) The three component volumetric average flow structure velocity surfaces, b) Volumetric flow structure obtained by three-dimensional background-oriented Schlieren method	32
Figure 3.1 Definition of a control volume (fixed in space).....	34
Figure 3.2 Surface forces acting on a surface element of the control volume	37
Figure 3.3 Isometric view of the CAD model of split air conditioner indoor unit	40
Figure 3.4 Front view of the CAD model of split air conditioner indoor unit.....	40
Figure 3.5 The air volume of the three-dimensional room model	41
Figure 3.6 Mesh structure of numerical model	42
Figure 3.7 Mesh structure of split air conditioner indoor unit	42
Figure 3.8 The position of the data point and plane.....	44
Figure 3.9 Velocity and temperature values for different number of elements	44
Figure 3.10 Velocity and temperature values for different number of iterations.....	46
Figure 3.11 Momentum and mass residuals of analyses a) Temperature: homogeneous, velocity: homogeneous, b) Temperature: homogeneous, velocity: PIV, c) Temperature: MIT, velocity: homogeneous, d) Temperature: MIT, velocity: PIV	49
Figure 3.12 Heat transfer residuals of analyses a) Temperature: homogeneous, velocity: homogeneous, b) Temperature: homogeneous, velocity: PIV, c) temperature: MIT, velocity: homogeneous, d) Temperature: MIT, velocity: PIV	50
Figure 3.13 Turbulence residuals of analyses a) Temperature: homogeneous, velocity: homogeneous, b) Temperature: homogeneous, velocity: PIV, c) Temperature: MIT, velocity: homogeneous, d) Temperature: MIT, velocity: PIV	51
Figure 4.1 Boundary conditions of outflow section: a) Temperature: homogeneous, velocity: homogeneous, b) Temperature: homogeneous, velocity: PIV, c) Temperature: MIT, velocity: homogeneous, d) Temperature: MIT, velocity: PIV	53
Figure 4.2 Average volumetric velocity profile at the outflow section of the split air conditioner.....	54

Figure 4.3 Penetration of outflow section of air conditioner indoor unit, a) Temperature: MIT, velocity: PIV, b) Temperature: MIT, velocity: homogeneous.....	55
Figure 4.4 Streamline visualization of mid plane of room: a) Temperature: homogeneous, velocity: PIV, b) Temperature: homogeneous, velocity: homogeneous.....	56
Figure 4.5 Velocity distributions at 1.70 m above ground of room: a) Temperature: homogeneous, velocity: PIV, b) Temperature: homogeneous, velocity: homogeneous.....	57
Figure 4.6 Temperature distributions at 1.70 m above ground of room: a) Temperature: MIT, velocity: PIV, b) Temperature: MIT, velocity: homogeneous.....	58
Figure 4.7 Temperature distributions at 1.70 m above ground of room: a) Temperature: MIT, velocity: homogeneous, b) Temperature: homogeneous, velocity: homogeneous.....	60

LIST OF TABLES

	Page
Table 2.1 Specifications of the SPIV system components.....	16
Table 3.1 Details of mesh independence study	43
Table 3.2 Details of iterations independence study	45
Table 4.1 The temperature values of the regions in Figure 4.6.....	59
Table 4.2 The temperature values of the regions in Figure 4.7.....	60



CHAPTER ONE

INTRODUCTION

1.1 Introduction

Split air conditioning systems stand out as an important tool in meeting the needs of small-scale summer and winter air-conditioning. The investigation of these devices in terms of flow conditions and temperature distribution is very important both in terms of energy efficiency and comfort. For energy efficiency, both indoor and outdoor units of split air conditioners need to be examined. However, considering the thermal comfort, the conditioned air flow structure and temperature distribution at the outflow of the air conditioner indoor unit should be examined.

Only the flow and temperature investigation at the outlet section of the air conditioner is not sufficient to examine the behavior of the device in the room. The shape of the room, the layout of the appliance, the furnishings in the room and the environmental conditions (such as the position and size of the windows, the ambient conditions, etc.) play a decisive role in the behavior of the flow from the appliance into the room. However, it is not possible to predict all of these parameters during production and to make the design in this direction. For this reason, flexible designs with different flow characteristics are tried to be made by taking from the most suitable design way for the general usage conditions.

1.2 Literature Survey

There are theoretical, numerical and experimental studies on the quality of indoor environments in the literature. Fanger (1972) studied the parameters affecting the thermal balance of the human body. As a result of these studies, an equation known as the comfort equation was proposed.

Fanger (1972) & Wargocki (1998) worked on indoor climates. In these studies, it was presented that indoor air velocity, indoor air temperature, indoor air pollution and flow patterns influenced on indoor climate.

Another parameter that is critical for indoor air quality is air pollution. Air pollution can be produced in the indoor environment as well as brought from the outdoor environment. Nero (1988) & Brohus (1997) have studied indoor air pollution. The parameters of these studies are the air pollution produced in the indoor environment, not the air pollution brought to the indoor from the open air.

A study by Awbi (1989) revealed how important thermal comfort and indoor air quality are. In this study, it was found that people spend 90% of their time in indoor. This shows that indoor air flow and temperature distribution are influential on humans and should be examined.

Besides as mentioned above theoretical studies, it is also available in experimental studies. While parameters such as temperature and velocity are analyzed, it is necessary to make measurements with large areas due to spatial and temporal variability. Conventional methods such as thermocouple, thermistor, hot wire anemometer, laser Doppler velocity meter and passive gas tracers are frequently used to measure air velocity and air temperature. These methods are capable of point measurement. Therefore, a large number of sensors and labour are needed to examine the entire room. Because of the disadvantages of conventional measurement techniques, the particle image velocimetry (PIV) method, which allows whole-field velocity measurement, is usually preferred for velocity measurement in the indoor environments. There are studies on point measurements and whole-field measurements in the literature.

Sun & Yang (2007) summarized the methods of studying the motion of air in a room. The methods used to obtain the velocity data were divided to be capable of point measurement and capable of whole-field measurement. The point-wise techniques include Pitot tube and rotating-vane anemometry, which are based on pressure

differential principles; hotwire anemometry, hot-film anemometry and hot-sphere anemometry, on heat transfer principles; ultrasonic anemometry (UA), on acoustics principles; and laser Doppler velocimetry (LDV), on Doppler shift principles. The whole-field techniques mainly include particle tracking velocimetry (PTV), particle streak velocimetry (PSV) and particle image velocimetry (PIV), which are based on optical principles.

Cao, Sivukari, Kurnitski, Ruponen & Seppänen (2010) investigated the turbulent jet flow into the ambient air from the active chilled beam in a climate chamber using PIV. The attached Plane jet with high turbulence intensity and low Reynolds number was investigated quantitatively and instantaneously with PIV.

In another PIV study, Meslem Nastase, & Allard (2010) achieved instantaneous velocity distributions of two different jets using PIV. It has been reported that cross-shaped jets perform much better than circular reference jets for passive control of air diffusing systems.

Another study on velocity measurement using the PIV method was performed by Karadeniz, Kumlutaş, & Özer (2013). The flow structures of the split air conditioner indoor unit were investigated in three-dimensional. Stereo PIV was used to obtain the three-dimensional flow structure. Inferences about the relationship between the fan casing, the device edges and the cross flow fan (CFF) were investigated from the obtained velocity profiles. In addition, the temperature distribution at the outflow section of the air conditioner indoor unit was visualized and temperature values were obtained by using the meshed infrared method which is developed in a three-dimensional version in the present study.

Methods of studying indoor parameters not only include experimental and theoretical methods but also a numerical simulation. Because of the cost and effort of the whole area measurement and the limitations of the point area measurement in the experimental methods, Computational Fluid Dynamics (CFD) is a method which is foreground to examine the indoor air environments.

The CFD method used for many years as a research tool for the indoor flow of a room (Nielsen, 1973; Nielsen, 1974; Jones & Whittle, 1992). There are many review studies that can show the historical development of the studies in which the airflow in the room was studied using the CFD method (Chow, 1996; Zhai, 2006; Nielsen, 2015).

Despite the fact that numerous studies which theoretical, experimental and numerical methods are applied separately are in the literature, the number of studies in which these methods are used together is limited. Karadeniz, Kumlutaş, Özer, & Kuru (2011) investigated the effect of different room geometries and device location on the distribution of conditioned air in the room. The velocity data obtained from the PIV experiment was defined as a boundary condition of a numerical model. Thus, the flow in the room were modeled in a more realistic.

1.3 Objective

The aim of this study is to define the values obtained from experimental data as boundary conditions in CFD program and to analyze these definitions parametrically. In the numerical model, the air velocity data obtained from the Particle Image Velocimetry (PIV) system positioned at the outflow section of the air conditioner were used as the velocity input. For the temperature input, the temperature data obtained using the Meshed Infrared Thermography (MIT) method were used. Thus, while the behavior of the indoor unit of the air conditioner in the room is numerically investigated, the boundary conditions defined on the outflow section represent more realistic situations.

In conventional CFD studies, all values in the defined boundary surface condition are considered equal across the surface. In these studies, homogeneous velocity and temperature values are defined as boundary conditions. For this reason, the information entered into the CFD program is one dimensional. In this study, unlike the literature, three-dimensional velocity and temperature data obtained from the experiments were defined as boundary conditions. In the literature, CFD studies are not able to define vector components of velocity at each point. In our study, the three-

dimensional and three-component velocity data obtained from the PIV experiment allowed defining vector components of velocity in CFD program. Thereby, both local and volumetric effects in the defined regions were defined as boundary conditions.



CHAPTER TWO EXPERIMENTAL STUDY

2.1 Particle Image Velocimetry (PIV)

2.1.1 History of PIV

The movement of liquids has attracted people's attention for years. The Italian polymath Leonardo Da Vinci (lived between 1452-1519) was the first person to begin visualizing flow structures. He drew flow patterns of flowing water and vortices of aortic valves. These drawings are shown in Figure 2.1 and 2.2.

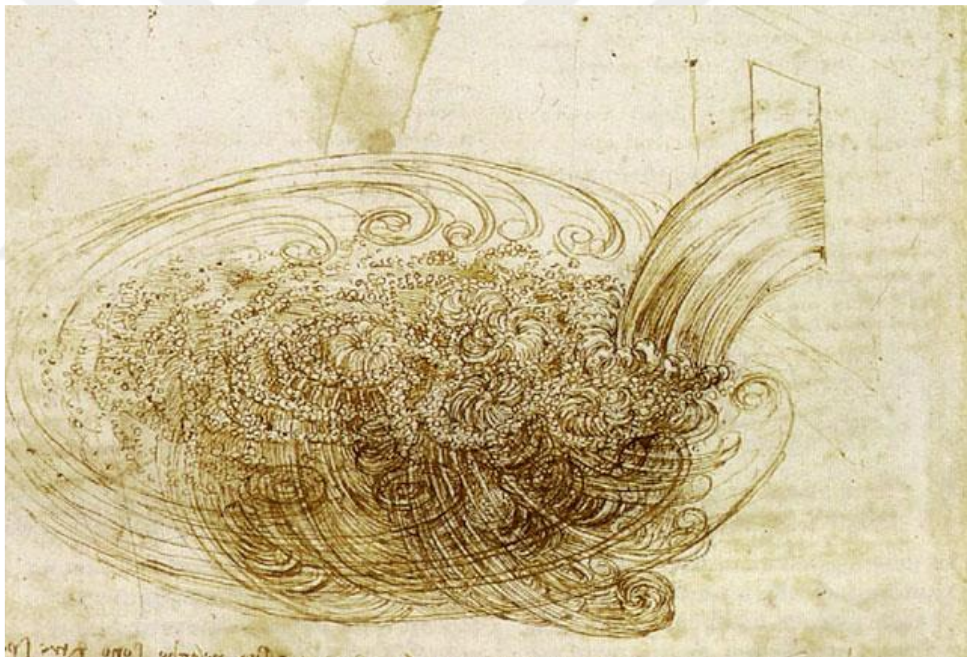


Figure 2.1 Leonardo da Vinci's "a free water jet issuing from a square hole into a pool" (Gad-el-Hak, 2000)

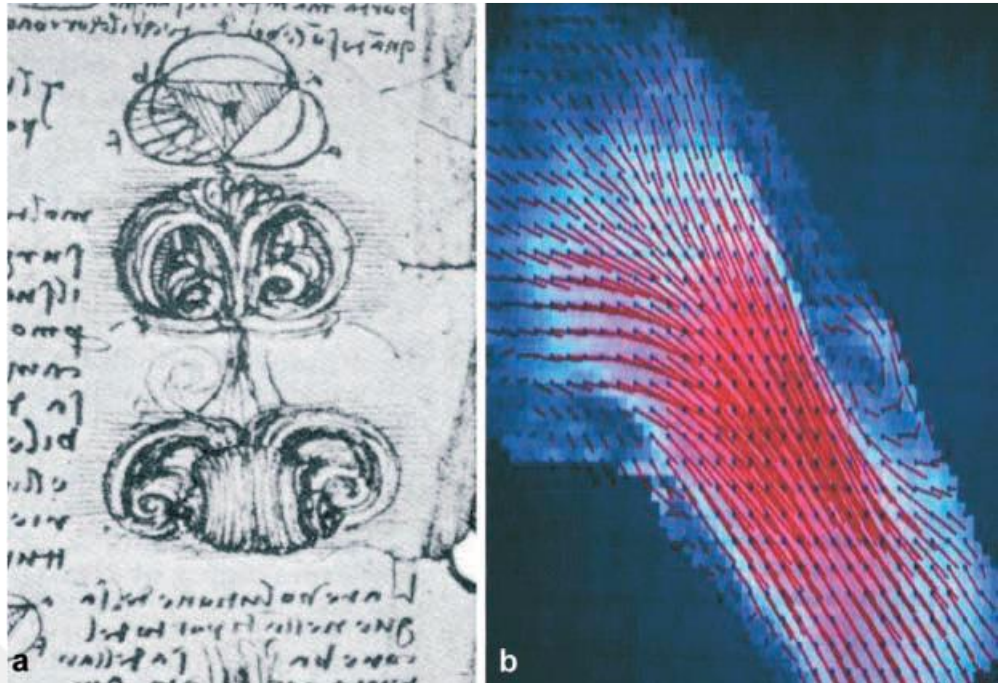


Figure 2.2 a) Leonardo da Vinci's aortic valve vortices, b) Velocity vectors from MRI in the left ventricular outflow tract (Gharib, Kremers, Koochesfahani & Kemp, 2002)

The method of adding fluid to the particle was applied by Ludwig Prandtl in the 20th century. Prandtl added mica particles to the flow to observe the flow in a water tunnel and studied the 2-D flow (Figure 2.3 and Figure 2.4).

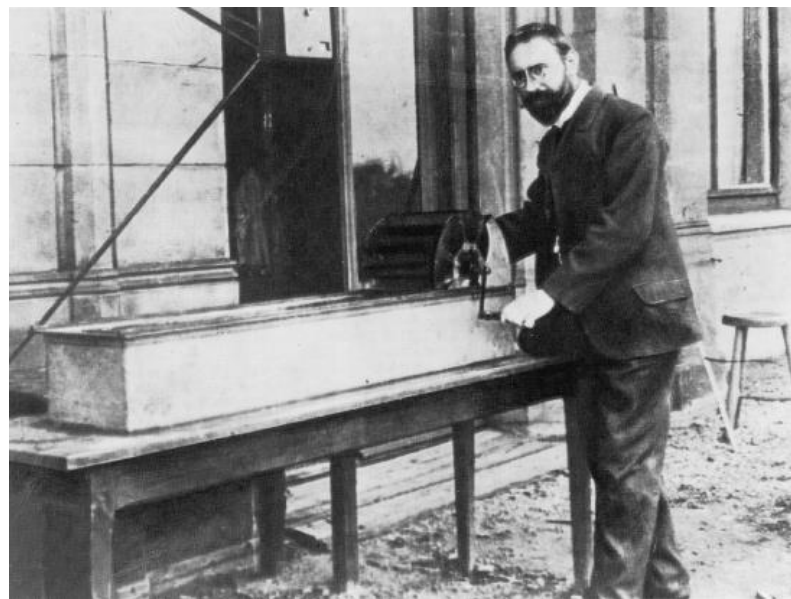


Figure 2.3 Ludwig Prandtl in front of his water tunnel for flow visualization in 1904 (Raffel, Willert, Wereley, & Kompenhans, 2007)

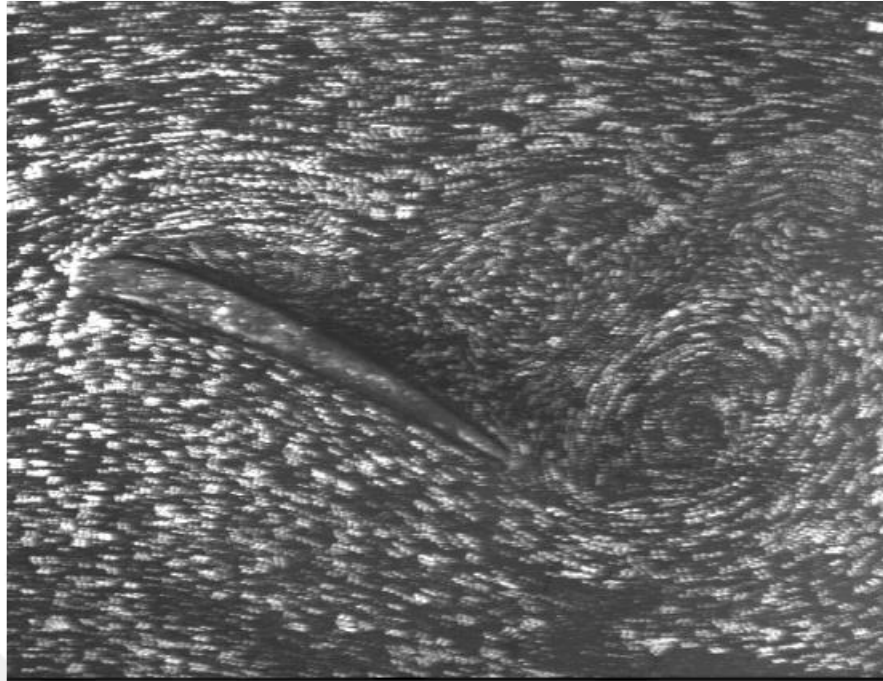


Figure 2.4 Separated flow behind wing, visualized with modern equipment in a replica of Ludwig Prandtl's tunnel (Raffel, Willert, Wereley, & Kompenhans, 2007)

Prandtl's works provide qualitative information about the flow. Therefore, these studies are not suitable for system design.

In the late 1970s, particle image velocimetry (PIV) development began with Laser speckle velocimetry experiments. In the 1980s, it was noticed that splitting the analysis area into interrogation areas made it easier to investigate the flow. With the development of laser, camera and computer technologies, PIV quickly developed and became digital. Today, PIV is a reliable experimental method and continues to evolve. Figure 2.5 shows the vector map of PIV experiment of Prandtl's tunnel shown in Figure 2.4.

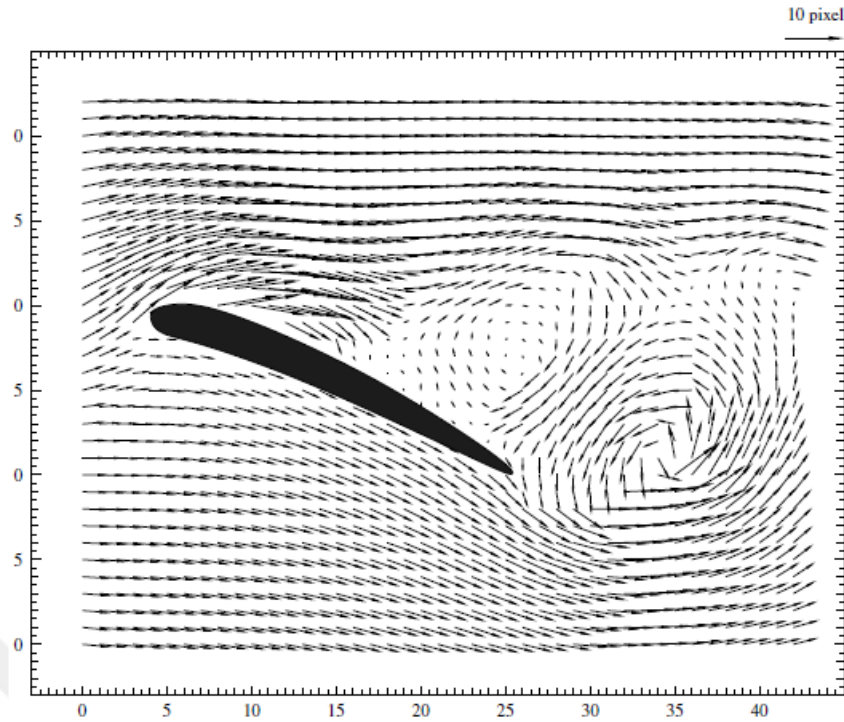


Figure 2.5 Vector map of instantaneous velocity field (Raffel, Willert, Wereley, & Kompenhans, 2007).

2.1.2 Methodology of PIV

PIV is a flow visualization method that can give both quantitative and qualitative results. Instantaneous velocity measurement of the flow can be performed using the method.

In PIV applications, the flow is seeded with tracer particles. In order to make the PIV experiment successful, the particles must be able to move coherently with the flow and reflect the light. The light reflection properties of the particles are critical for imaging by infrared cameras.

The particles are illuminated by a powerful light source as they pass through the investigation area. This light source illuminates the particles by forming a light sheet. Different light sources (LED etc.) are available in the literature, but lasers are widely used because of their practical ability to form a light sheet.

The light sheet is important for determining the positions of particles in PIV measurements. It can also be explained that a single camera can only create 2D data. If a third dimension component of data is needed, at least one more camera located at different angles is needed. The main difference of PIV applications from other flow measure method like laser Doppler velocimetry and hot-wire anemometry is the ability to produce 2D or 3D data instead of point data.

High shutter speed is used in PIV applications. For this reason, clearness and sharpness are important in the images. This is also why high power light sources are used.

The position of the particles in the image couples obtained at high shutter speed is compared with the computer program. The displacement of the particles in the two images is divided into time between images capture to obtain the velocity data. In PIV applications, the investigation areas are separated by the interrogation areas and the position of the particles in these areas is determined by cross-correlation in the second image.

2.1.3 Components of PIV

A conventional PIV setup consists of five main components. These are the camera and lens setup, the laser as light source, the synchronizer that provides the relationship between the laser and the cameras, the fog generator that seeding the flow with tracer particles, and the computer on which the images are processed.

While these main components exist in each PIV device, different features of component models can be had in different applications.

2.1.3.1 Seeding Particles

As mentioned in previous chapters, PIV is an indirect measurement method. In PIV applications, the seeding particles are displayed by cameras. Therefore, the seeding particles are important component of PIV systems.

The seeding particles must follow the flow behavior in harmony with the fluid. Otherwise, only the data of the particles which do not move in accordance with the flow is obtained, not the correct data of the flow.

While the actual particle choice is dependent on the nature of the fluid, generally for macro PIV investigations they are glass beads, polystyrene, aluminum flakes or oil droplets (if the fluid under investigation is a gas). Besides, the refractive index of the particles must be different from the flow. Therefore, the laser will be scattered from the particle to the camera.

The dimensions of the particles are also important for the success of the experiment. The particles must be large enough to reflect a large portion of the light coming from the laser, small enough to follow fluid motion within the response time. In PIV applications, the seeding particles 10 to 100 micrometers in diameter are used.

In post-process analysis, cross-correlation is used to measure displacement. To achieve this, it is necessary to distribute the particles at the proper density. In Figure 2.6, different particle densities are shown. The particle density shown in the image (b) is suitable for PIV applications. However, as in picture b, the infrequent distribution of particles can not support speed information. Image (c) has a very dense distribution, so the questioning areas can not be determined correctly.

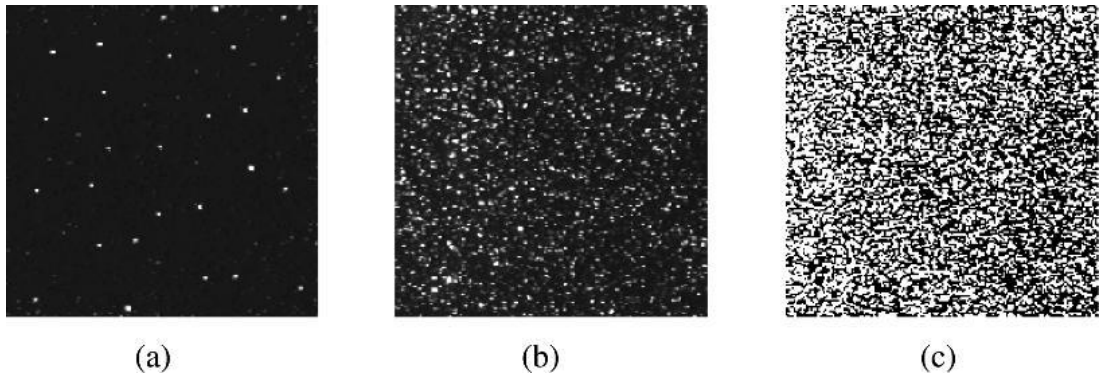


Figure 2.6 Different particle distribution densities (Raffel, Willert, Wereley, & Kompenhans, 2007)

2.1.3.2 Cameras and Lenses

To perform PIV analysis on the flow, two exposures of laser light are required upon the camera from the flow. Cross correlation method is applied between 2 images obtained for flow analysis. In this method, the same particles within the interrogation areas are determined between 2 images. So we get 2 views of displacement and velocity data. In order to success of this method, the time between two image should be as possible as short due to the flow rate. Otherwise, the particles that we see in the first laser pulse may be out of sight in the second image. Therefore, high speed cameras are used in PIV applications.

The images of the particles in the interrogation area should be focused and visualized correctly. The select of the correct lens is important to achieve this. The image is formed close to the lens, inverted, laterally reversed and real. The image plane in which this image is formed is termed the principal focal plane (F). Focal length also has a relation with the angle of view (AOV). AOV gets larger as focal length shortens. This phenomenon is shown in Figure 2.7.

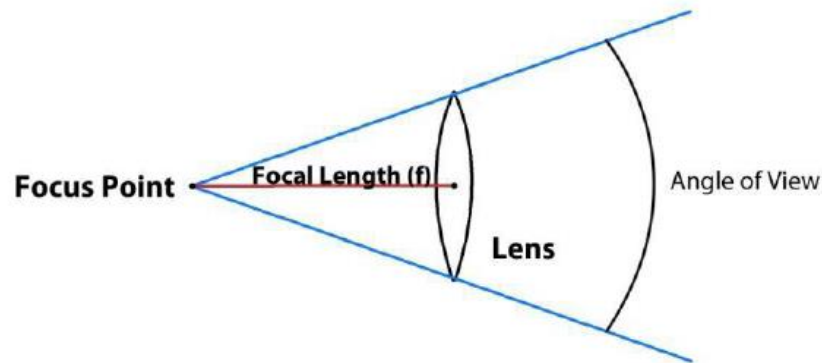


Figure 2.7 The focal length and angle of view (AOV)

There are 3 different lenses depending on focal length and vision. These are normal lenses, telephoto lenses with larger focal lengths than normal lenses, and wide-angle lenses with larger AOV. Since wide angle lenses can cause perspective errors, they are not preferred for use.

2.1.3.3 Laser and Optics

ND: YAG (Neodymium Yttrium Aluminum Garnet) lasers are commonly used in PIV setups. The use of ND: YAG lasers is due to their high light intensity. These lasers emit light at a wavelength of 1064 nm. Cameras are often sensitive to the blue-green part of the spectrum. Therefore, the wavelength of the ND: YAG laser is halved by the harmonic generator. Another advantage of this is that it allows the laser beam to be seen with green color in the measurement area.

The laser optics consist of a spherical lens and a lens of silicone. The task of the cylindrical lens is to expand the laser, and the task of the spherical lens is to make the laser a thin layer. But the spherical lens cannot compress the laser layer into an actual 2-dimensional plane. The minimum thickness of the laser plane is at the focal point of the spherical lens. This distance gives information about the distance at which the experiment is to be carried out.

2.1.3.4 Synchronizer

The synchronizer acts as an external trigger for both the camera(s) and the laser. Unlike the past, most systems in use today are digital. The task of the synchronizer is to provide timing between firing of laser and CCD camera image acquisition. The accuracy of the timing is around 1 ns. So that the image is taken during the laser pulse and the correct calculation is made between the two laser pulses. the flow rate is calculated by this information.

2.1.4 PIV Setup Used in Current Study

Each study has a different investigation area and different characteristics of this area. Therefore, PIV setups can alter for the needs of the study. Many PIV methods have been developed to provide solutions for different needs. Some of these are stereoscopic PIV (SPIV), dual plane stereoscopic PIV, panoramic PIV, endoscopic PIV (EPIV), micro PIV, holographic PIV, scanning PIV and tomographic PIV.

In the present study, stereoscopic PIV was used. In the basic PIV, two-dimensional velocity measurement of the investigation area can be done. The SPIV method can give the three-dimensional velocity data of investigation plane. A schematic representation of the SPIV method is given in Figure 2.8.

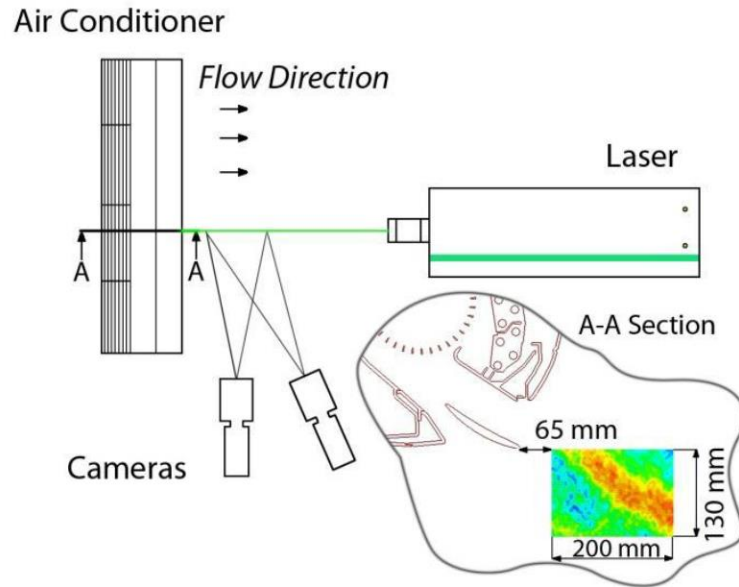


Figure 2.8 The schematic of SPIV setup

The PIV setup of the current study is shown in Figure 2.9. Figure 2.9 shows that the seeding particles do not disperse homogeneously into the flow, but the cameras point to the same area of view.

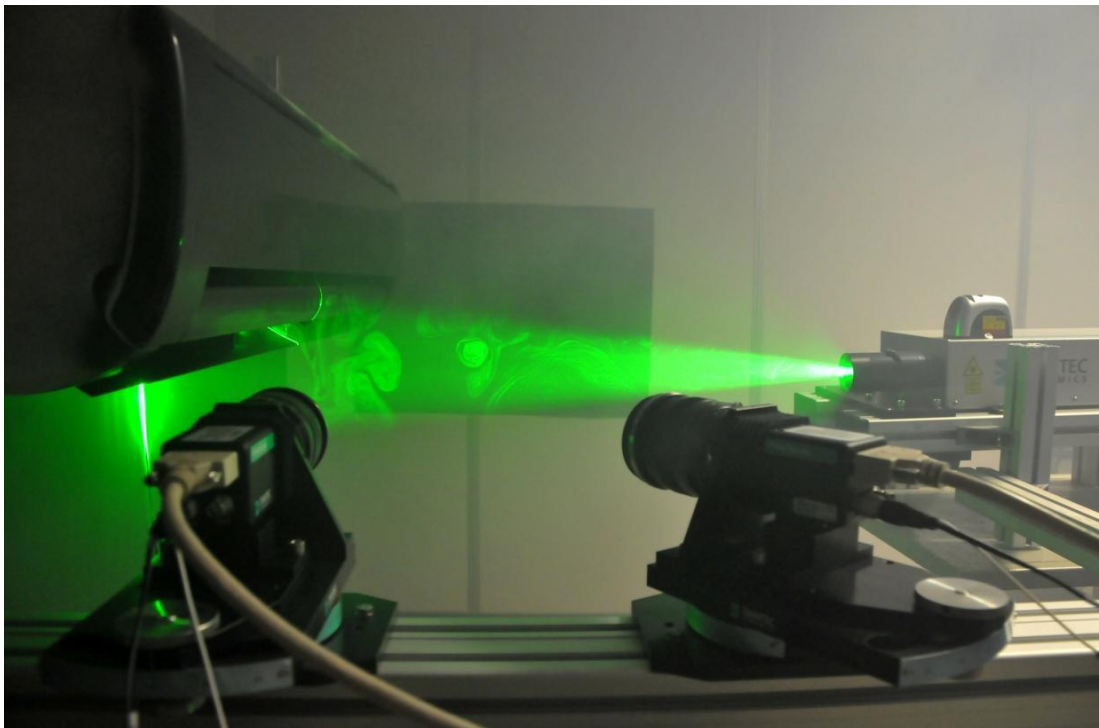


Figure 2.9 Photography of the SPIV setup

Another issue that is critical for SPIV is the calibration. As shown in Figure 2.10, the camera on the right looks at the calibration target with an angle, and specifies that the points on the left image correspond to the points on the right image.



Figure 2.10 The calibration target with both cameras

As mentioned earlier, the PIV components may vary according to the cases. The components of SPIV setup that used in the study are shown in Table 2.1.

Table 2.1 Specifications of the SPIV system components

Components	Specifications
1) Laser	135mJ, 15Fps double pulse ND:Yag Laser
2) Camera & Lens	Flow Sence Mark II, 4 MPx, square sensor camera. 60mm f 2 Zeiss Planar Macro Lens
3) Synchronizer	Dantec Dynamics Synchronizer Box
4) Fog Generator	Safex fog generator, with extra clean fog fluid
5) Computer	Dell T7500 work station, 12 GB ram, Raid 0

2.2 Meshed Infrared Thermography (MIT)

Infrared imaging can only measure the temperatures of objects that are opaque at the infrared wavelength and radiate with definitive emissivity coefficient. However, the gases are transparent in the infrared wavelength (7-13 μm). For this reason, the

infrared camera cannot directly determine the temperatures of the gases. Measurement screen methods are used in the literature to solve this problem.

2.2.1 Infrared Thermography

Infrared radiation was discovered as a form of radiation beyond red light by the British scientist William Herschel, who lived in the 19th century. These rays are mainly used for thermal measurement from the past to the present (Herschel, 1800). One of these measurement methods is an infrared thermography. Infrared thermography, thermal imaging, and thermal video are examples of infrared imaging science. The radiation in the long-infrared range of the electromagnetic spectrum (roughly 9,000–14,000 nanometers or 9–14 μm) can be detected by thermographic cameras. Thus, thermographic cameras produce images of that radiation. According to the black body radiation law, infrared radiation is emitted by all objects on the absolute zero. Thus thermography makes it possible to see one's environment with or without visible illumination. The amount of radiation emitted by an object increases with temperature; therefore, thermography allows one to see variations in temperature. The hot object captured by the thermographic camera stands out against the cold surroundings so that people or animals can easily be seen day or night. Because of this feature, the thermographic camera has a widespread use, especially in the military field.

The thermography, which is increasing in use rapidly in the last half a century, serves many fields. Thermography is widely used in many areas like thermal insulation in buildings, air conditioning systems, to find people in a fire, detection of errors caused by overheating etc.

The thermographic camera is similar to a normal camera in terms of operation and appearance. CCD and CMOS sensors are used for visible light. These sensors are not sensitive to the thermal region of the infrared spectrum. Thermal imaging cameras use specialized focal plane arrays (FPAs) that respond to longer wavelengths (mid and

long-wavelength infrared). The most common types are InSb, InGaAs, HgCdTe and QWIP FPA.

Current technology thermographic cameras often use low cost, uncooled microbolometers as FPA sensors. A microbolometer is a specific type of bolometer used as a detector in a thermal camera. Infrared radiation with wavelengths between 7.5-14 μm strikes the detector material, heating it, and thus changing its electrical resistance. This resistance change is measured and processed into temperatures which can be used to create an image. Unlike other types of infrared detecting equipment, microbolometers do not require cooling. The resolution of the microbolometers is usually much lower than the optical cameras. There are common 160x120 and 320x240 resolution versions on the market. It is available in 1024x768 resolution thermal cameras, but they are very expensive.

2.2.2 Emissivity

The ability of a material to emit thermal radiation is called emissivity. Each substance has an emissivity value between the theoretical 0.00 (completely non-emitting) and theoretical 1.00 (completely emitting). An example of a substance with high emissivity would be asphalt, with an emissivity coefficient of .98.

Black body is an object that does not actually exist and radiate infrared radiation at its contact temperature in theory. For example, if the black body temperature is 70 $^{\circ}\text{C}$ degrees, the radiation of black body is 70 $^{\circ}\text{C}$.

The infrared radiation of normal objects will be less than the contact temperature because there is no such thing as a perfect black body. The rate (percentage) of emission of infrared radiation will thus be a fraction of the true contact temperature. It is called emissivity.

The long wavelength emissivity of some objects may be different than the mid wavelength emissivities. The emissivities of some objects may change as a function of temperature.

The object emissivity value should be entered into the camera in order to accurately measure an object temperature with the thermographic camera. Thus, the camera's algorithm uses this emissivity value to calculate a temperature close to the actual temperature of the object.

It is a more accurate approach to testing the emissivity of an object than to determine emissivity values from tables. For this test, a thermographer may apply a standard material of known, high emissivity to the surface of the object. This material may be an industrial spray produced for this purpose or standard black insulation tape which has an emissivity about 0.97. Then, the object with the emissivity level on the imager set to the value of the test material thus a temperature can be obtained. The measured value will give the accurate temperature. The temperature can then be read on a part of the object not covered with the test material. If the temperature values are different from each other, the emissivity value can be changed until the temperature value obtained in the second reading is equal to the first reading. The emissivity test may be impossible in difficult and hazardous situations. In these cases, it is better to set an emissivity value with help from the tables.

2.2.3 Two Dimensional Meshed Infrared Thermography

The measurement screen method is based on the display of a solid target placed in the gas media with an infrared camera. Heat transfer occurs by convection between the gas media and the target. So we can determine the temperature of the gas media by means of the temperatures we have obtained over the solid target. It must be noted that this method measures gases temperature indirectly therefore the success of the measurement is depending on the heat transfer mechanism between the measurement screen and the gas. In this sense, there are different types of measurement screen targets in the literature.

These measurement screens are generally sheets or papers about a millimeter thickness with low thermal conductivity (Anderson, Hassani, & Kirkpatrick, 1991; Cehlin, Moshfegh, & Sandberg, 2002). These screens are placed inside the stream and a temperature distribution occurs on the surface with convective heat transfer. As the sheet or paper is thin, the temperature distribution detected by the infrared camera reflects the temperature distribution of the stream. However, as these sheets with vast surface area exchange heat via radiation with surrounding surfaces, the environmental impact shall be calculated and differentiated from the obtained results. In addition, as the measurement screen provides a barrier within the stream, it can only be applied to low velocity flow not to disrupt the general nature of the stream. Beside these, there is another measurement screen method which is proposed as the “Meshed Infrared Thermography (MIT)” (Karadeniz, Kumlutaş, & Özer, 2013). In this method; the temperature is measured by the spheres that are placed with pre-determined intervals on the nylon threads that are stretched between the two edges of a frame that is placed in the flow to have minimum effect on the flow. The benefits of the MIT method are minimal disruption on the flow that is an ignorable and convenient measurement of the planar heat distribution with the utilized spheres. The schematic of the MIT experiments is shown in Figure 2.11.

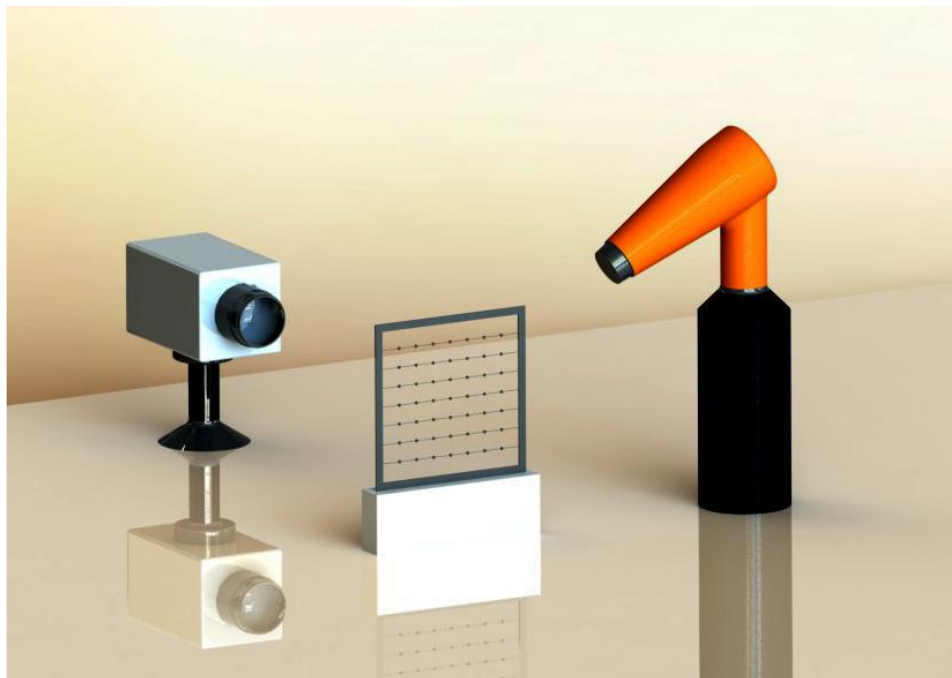


Figure 2.11 The schematic of the MIT experiments (Özer, 2011)

The flow effects of the MIT method and other measurement screen methods are shown in Figure 2.12.

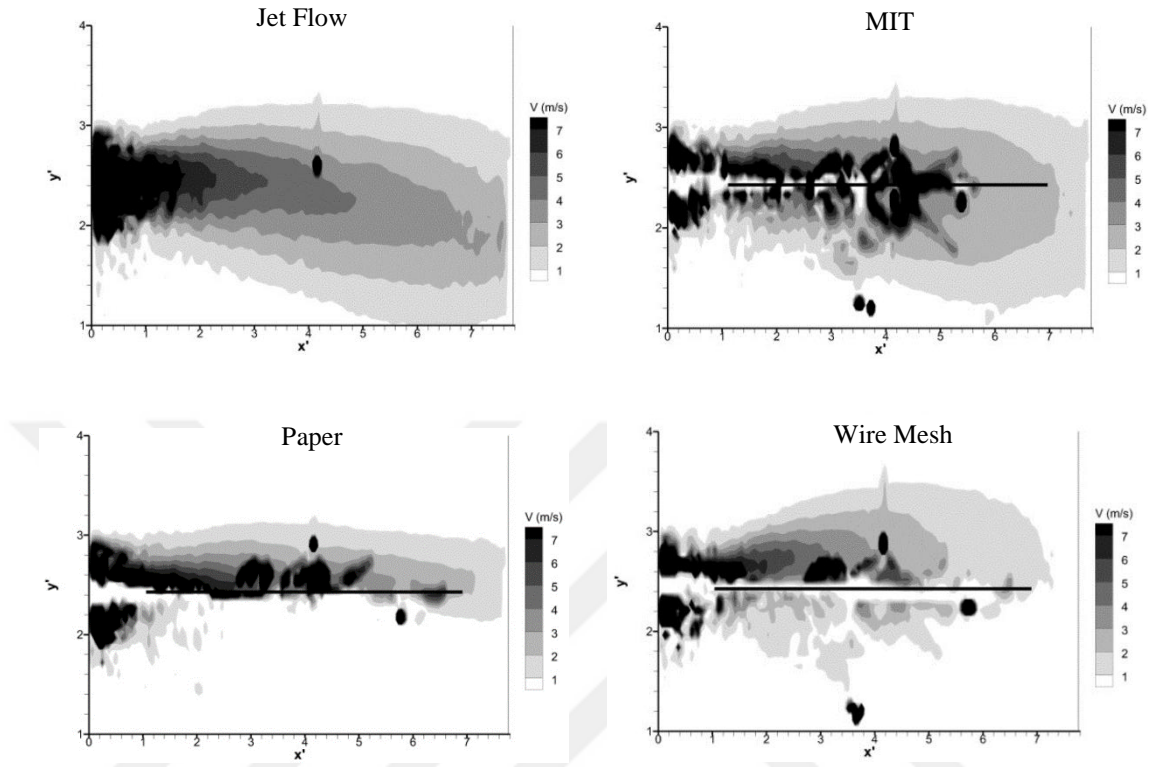


Figure 2.12 Velocity distribution for jet flow and measurement screens (Karadeniz, Kumlutaş, Özer, Kılıç, & Ünsalan, 2013)

2.2.4 Validation Experiment of Meshed Infrared Thermography

The validation experiment of the Meshed Infrared Thermography (MIT) method is presented in the literature (Özer, 2011). A blower with an output temperature of 50⁰ C and an output velocity of 5 m/s was used in the verification experiment and the MIT target was positioned in the jet air. The image of the validation experiments is shown in Figure 2.13.

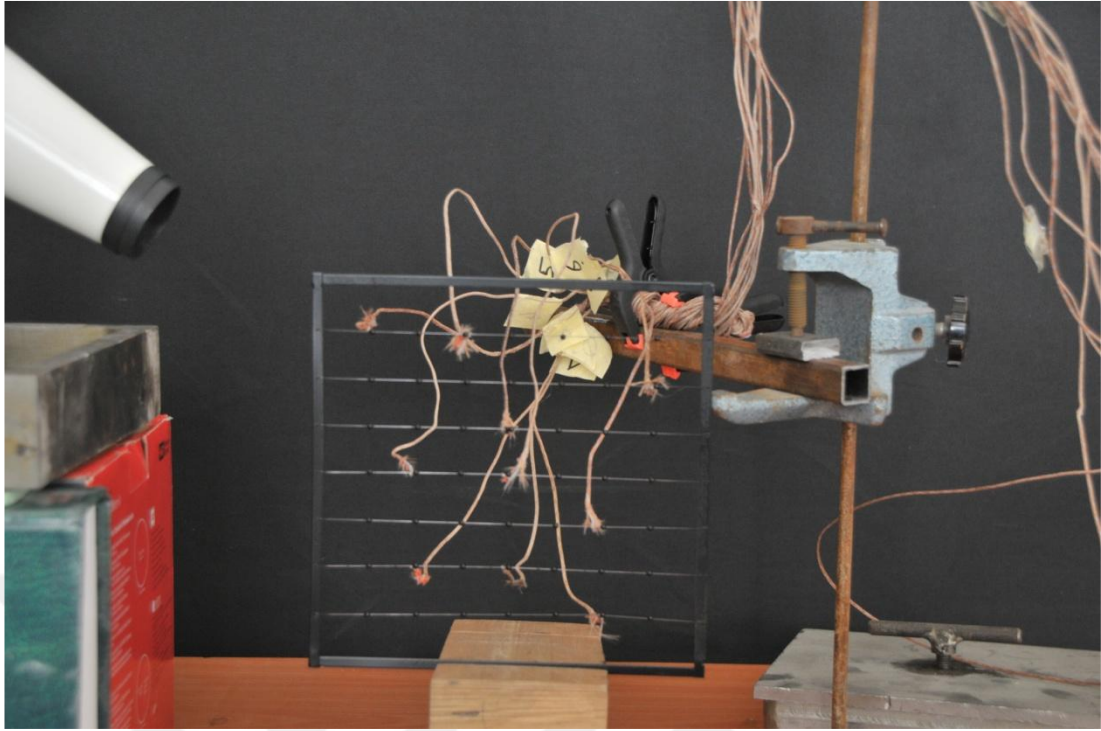


Figure 2.13 The image of the validation experiments (Özer, 2011)

The thermocouples previously calibrated in the water bath were placed at specific points on the MIT target. The position of the placed thermocouples is shown in Figure 2.14.

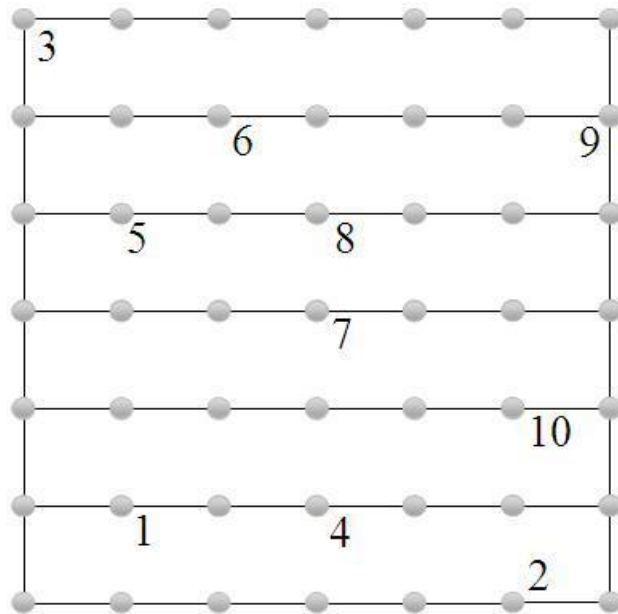


Figure 2.14 The position of thermocouples (Özer, 2011)

The values obtained from these points were compared with the values obtained by applying the MIT method. Temperature data was obtained from thermocouples at points 1, 3, 6 and 10. Instantaneous temperature data were obtained from the same points by the MIT experiment. Thermocouple and MIT experimental data were presented as comparative in Figure 2.15. In Figure 2.15, Ta represents the ambient temperature.

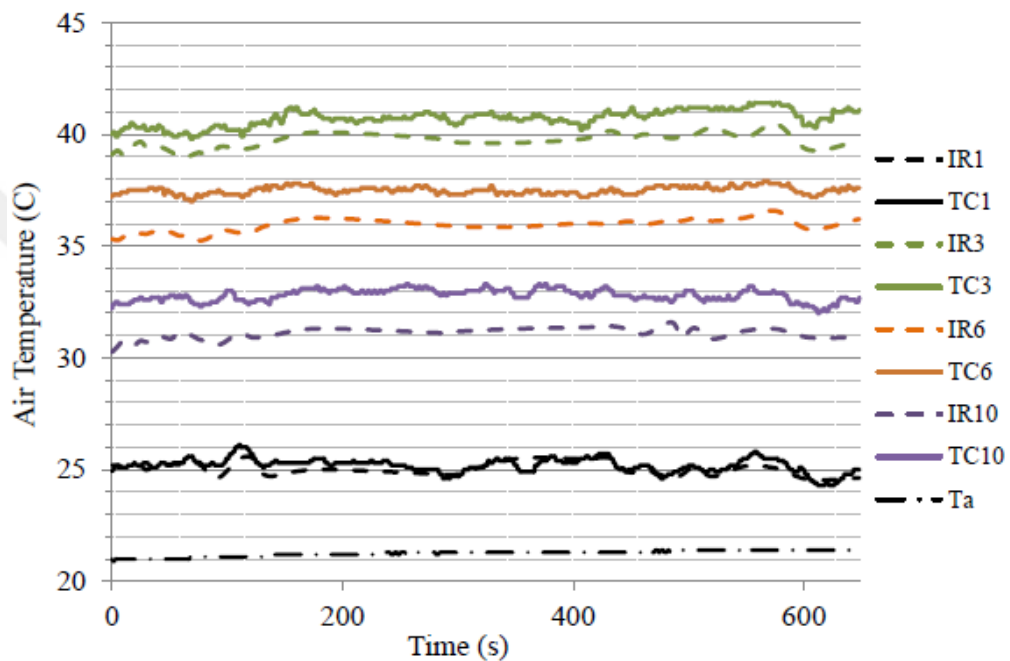


Figure 2.15 Steady state temperature measurements by PIIT (IR) and thermocouples (TC) at different points on the measurement mesh (Özer, 2011)

The absolute difference between the averages of these instantaneous temperature values on individual points and averages of the corresponding thermocouple data is between 0.15 and 2.7 C and standard deviation of the absolute differences for all points is 0.68 C.

This validation, which is also acceptable in the three-dimensional application of the MIT method, indicates that the method is acceptable and adequate for flow visualization and temperature determination.

2.3 Alternative Flow Visualization Method: Three-Dimensional Background Oriented Schlieren Method (3DBOS)

The background-oriented Schlieren (BOS) method is a current developing method of flow analysis that allows the flow to be visualized using the refractive index effect of the density differences contained in the fluid. Image waving in the background due to the hot flue gas from the flue or the car exhaust can be given as an example of this phenomena. Gladstone-Dale equation (Equation 2.4) gives the relation between refraction index (n) and density (ρ) (Venkatakrisnan & Meier, 2004).

$$\frac{n-1}{\rho} = G(\lambda) \quad (2.1)$$

In the implementation of the method, the background of the flow area to be examined must be a textured surface. These textured surfaces may be natural or artificial. To guarantee the success of the experiment, it is recommended that the background texture is non-repetitive and random. In the current application of the method, the background is created by the computer. The textured background that is created should have high spatial detail and contrast to ensure the success of the experiment.

The camera must be placed perpendicular to the background to visualize the flow field. It is also recommended that the camera lens shouldn't be a wide angle lens to prevent additional perspective distortions. If the lens used does not have the mentioned features, the problems in the obtained images can be solved by digital image processing methods.

A reference image is recorded before the experiment (before the density difference occurs). Then the experiment is initiated so that the density difference originating from the flow is formed between the camera and the background. In this stage, the density difference causes the light to be diffracted with an angular deviation, resulting in a different view from the reference image. This situation is shown in Figure 2.16.

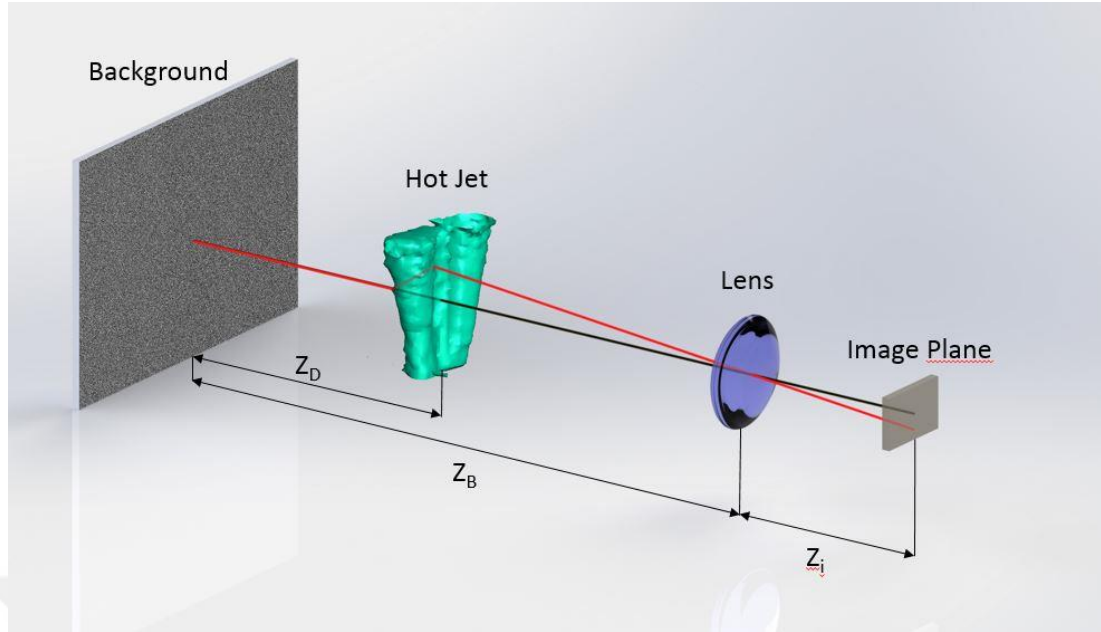


Figure 2.16 Schematic representation of the BOS method (Özer, Kumlutaş, & Yücekaya, 2017)

The light shown in black in Figure 2.19 represents the path that the light travels without exposure to the density difference, while the light indicated by red represents the path followed by the light that is refracted by the density difference. The distance indicated by Δy shows the difference between the reference image of the same point and the image taken during the experiment. In Figure 2.19, Z_D represents the distance between the background and the density difference, Z_i represents the focal distance, and Z_B represents the distance between the background and the camera lens.

The experiment and reference images are taken and the passed to the post-processing. At this stage, cross-correlation between the reference image and the experimental image is applied. This process is performed between the reference image and all the experiment images.

In the first step of the cross-correlation process, the reference image is divided into interrogation areas. Then the image obtained during the experiment is compared with the reference image in terms of position information. If the position of the image obtained during the experiment is the same as the position of the reference image ($\Delta y = 0$), this means that the incident rays are not subjected to any refraction, so there is no density difference on the ray path. The areas that have a difference between the two

locations indicates that they are reflected. By marking these areas, the flow structure can be determined. An experimental result of a jet flow is shown in Figure 2.17 (Özer, Kumlutaş, & Yücekaya, 2017).

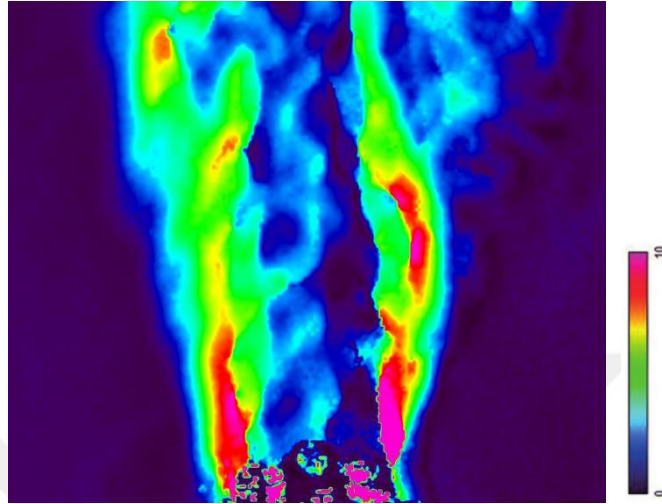


Figure 2.17 The result of the hot jet flow by BOS method (Özer, Kumlutaş, & Yücekaya, 2017)

In Figure 2.20, a jet cross section is shown. The color codes on the figure represent the displacement between two pictures on the pixel-by-pixel basis. The dark blue color represents no pixel-based displacement, while the other colors towards the purple color represent the displacement amount.

It should be noted that the result obtained from Figure 2.17 is a qualitative result. The visualized pixel-based displacement does not contain any velocity or temperature data as it provides information about the structure of the flow.

The single camera used in the implementation of the background-oriented Schlieren method provides information about two component positions, horizontally and vertically. This allows only the planar projection of the density distribution of the volumetric flow structure to be viewed. Therefore, the background-oriented Schlieren method can be considered to be useful in studying two-dimensional or radial symmetric systems, but insufficient to examine the volumetric flow structures in which the third dimension components are important.

In order to examine the mentioned volumetric flow structures, the "three-dimensional background-oriented Schlieren" method, which is the subject of the present section of the study, has been developed.

At least three components are needed in order to obtain the volumetric measurement. When a camera is thought to provide information about only two components, at least two cameras are required to display the three-dimensional flow structure. In the present study, three cameras were used to increase the detail of the obtained volumetric data. The camera is perpendicular to the selected x-y plane and the second to the y-z plane. The third camera is positioned between the other two cameras to form an angle of 45 degrees. The backgrounds which are one of the main components of the method are located on the other side of the flow to be investigated. The experimental setup is shown in Figure 2.18.

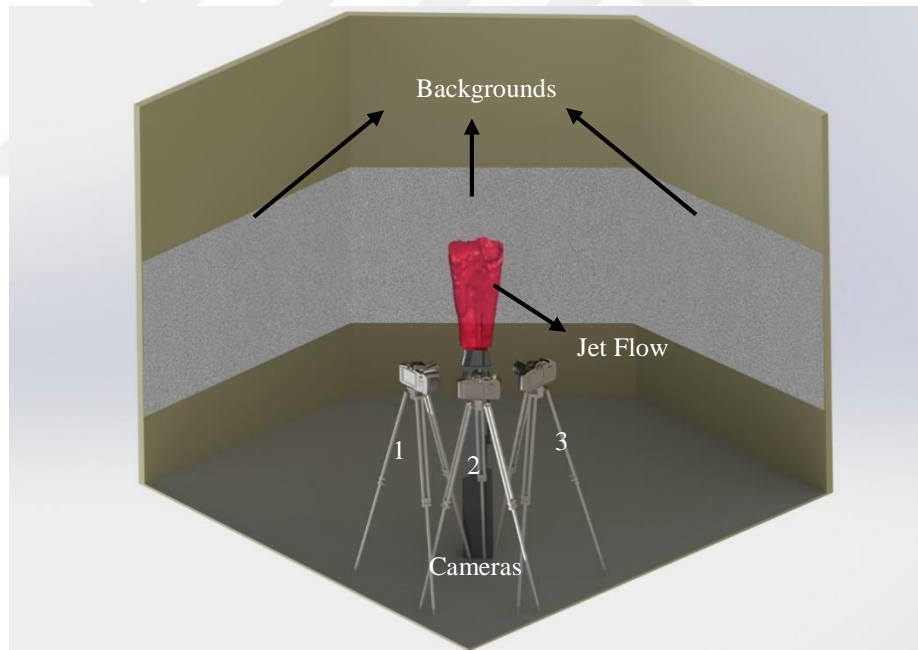


Figure 2.18 The experimental setup of 3DBOS method (Özer, Kumlutaş, & Yücekaya, 2017)

In the implementation of the three-dimensional version of the method, reference images are taken at the initial stage (before the density difference occurs). However, unlike the two-dimensional application of the method at this stage, it is necessary to take a calibration image to cover the viewpoints of the cameras. A calibration target placed in the flow area to be investigated is used to capture this view. The planar results

obtained after the completion of the experiment are made volumetric with the position information from these calibration images. Volumetric data in the present study were obtained using post-processing software.

2.4 Results of Experimental Study

Basically, the advantage of PIV is that the whole flow area can be investigated at the same time. In order to better evaluate this present advantage, there is a study in the literature about the creation of volumetric three-dimensional average velocity vectors (Karadeniz, Kumlutaş, & Özer, 2013).

In order to obtain the volumetric three-dimensional average velocity distribution, the system needs to be examined at certain gaps. The device was placed in a traverse system so that the device can be properly offset at these gaps. One of the cameras was positioned so that the flow generated by the device was viewed from the opposite side and angled. The laser was positioned so that the jet flow can be seen from the opposite side, providing the illumination needed for the cameras. The jet flow was scanned in 11 planes. In each investigated plane, two pairs of images were taken with two cameras. The processing of these image pairs yielded average planar three-component velocity distribution maps. There are 11 PIV images of outflow section scanned from 0 to 825 mm from the Z axis. The image at $z = 165$ is given in Figure 2.19 as an example.

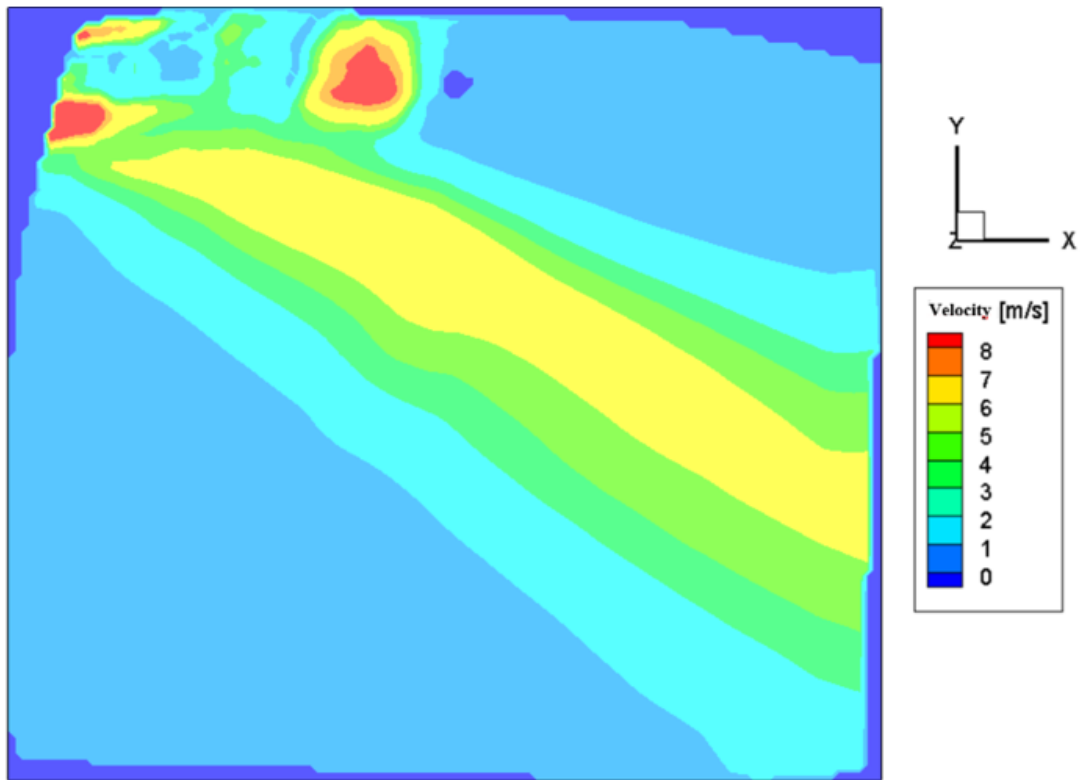


Figure 2.19 PIV image at $z = 165$ mm

The volumetric data generated from the data obtained from the planes are shown in Figure 2.20.

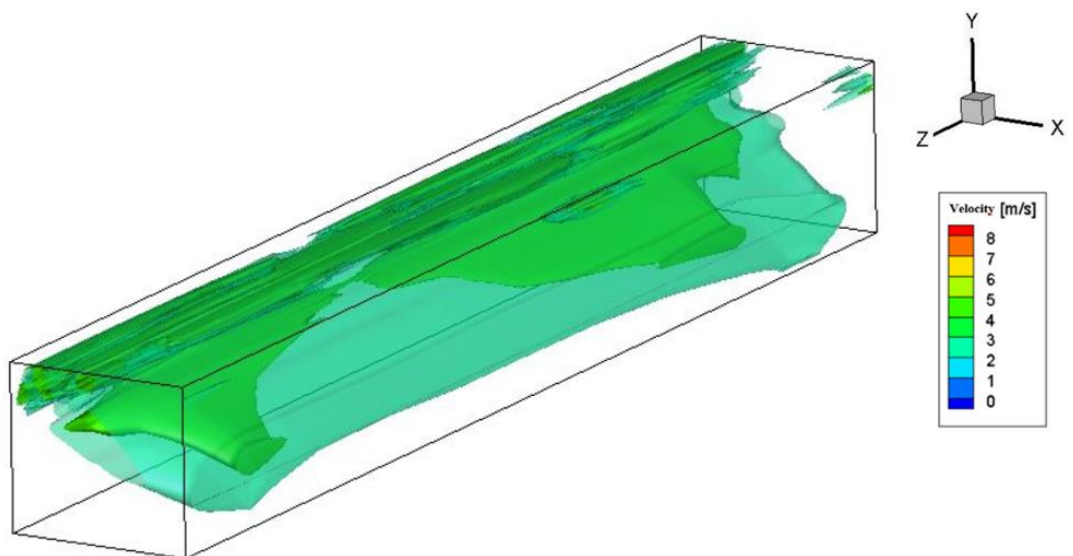


Figure 2.20 The three-component volumetric average flow structure obtained by the PIV method

A matrix was created with the values obtained in MIT method. The visualization of the matrix result can be seen in section 4, Figure 4.1-c and Figure 4.1-d.

Another experimental method used in this study, the developed "three-dimensional background-oriented Schlieren" method was applied to hot jet flow.. The measured jet outflow section dimensions are 120 mm x 28 mm. The average outlet temperature of the jet flow is 42 °C. For the examination of the jet flow, a mechanism consisting of three cameras was set up as shown in the Section 2.1.3 (Figure 2.20). In the experiment, end-user mirrorless cameras were used. The distance to the jet center of the cameras is 40 cm. The distance between the placed background and the jet center is 127 cm. The planar results obtained in the experiment are presented in Figure 2.21.

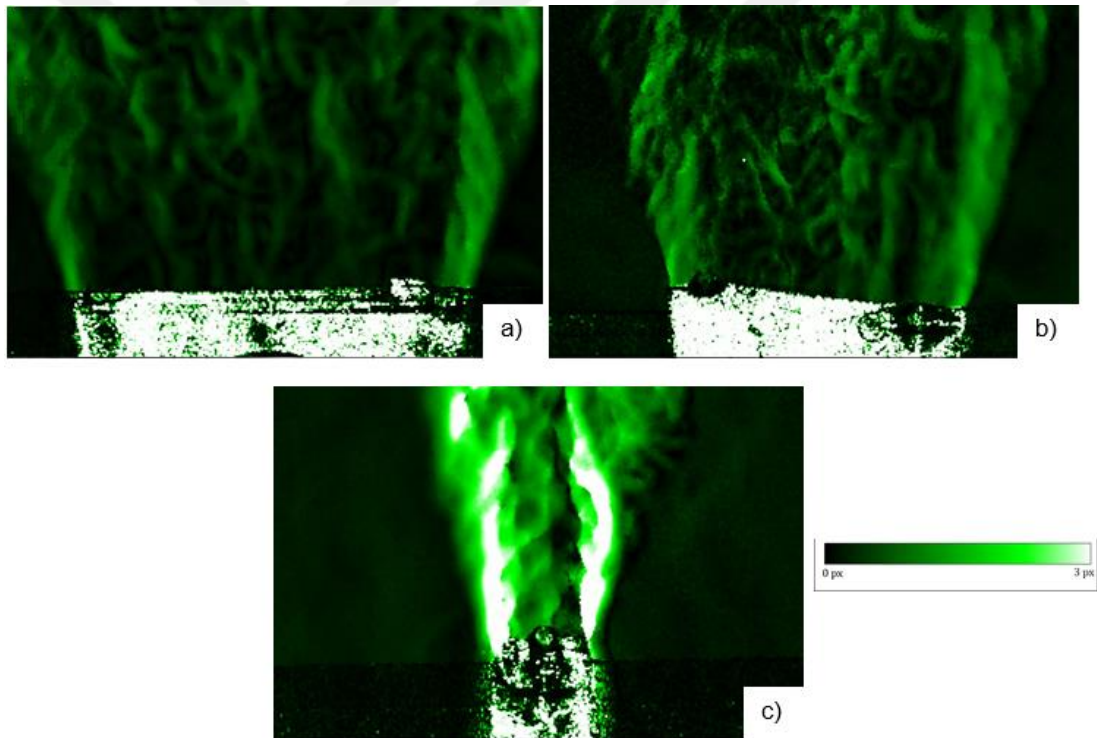


Figure 2.21 a) The result of the background-oriented Schlieren method obtained from the camera-1, b) The result of the background-oriented Schlieren method obtained from the camera-2, c) The result of the background-oriented Schlieren method obtained from the camera-3 (Özer, Kumlutaş, & Yücekaya, 2017)

It can be seen that when the images in Figure 2.24 are evaluated, the boundary regions of the jet are clearly determined. When the images obtained from different

cameras were evaluated, it was found that the density differences can be seen more clearly in the image taken from the narrower section of the flow. The reason for this is that the surfaces of the areas with density difference in the center were located parallel to the camera. Therefore, the rays coming from these regions arrive at the camera with less refraction or without refraction. In addition, the background-oriented Schlieren data obtained from the three cameras were placed according to the calibration data and converted to volumetric data by interpolation in the special software. The obtained volumetric data is shown in Figure 2.22.

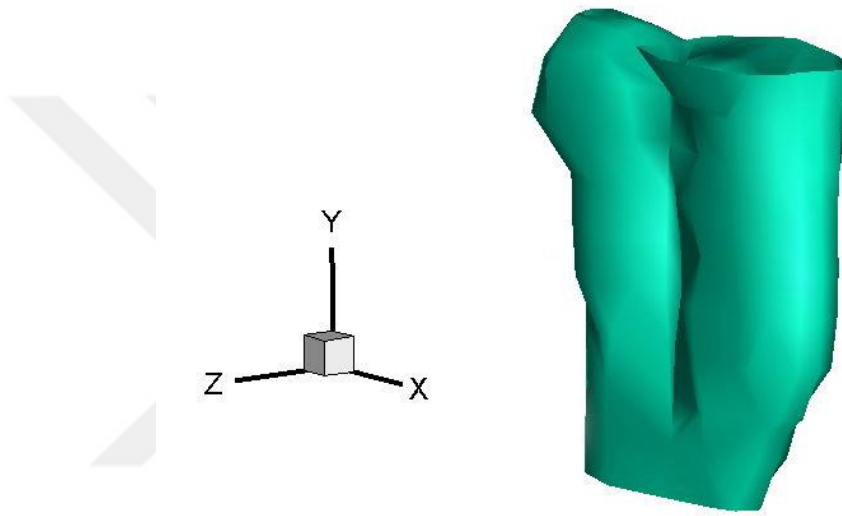


Figure 2.22 The result of 3DBOS method (Özer, Kumlutaş, & Yücekaya, 2017)

The same jet flow was also investigated by the PIV method. A volumetric 3D velocity distribution was obtained in the computer environment of PIV data. The three component volumetric average flow structure velocity surfaces obtained by the PIV method are shown in Figure 2.23-a.

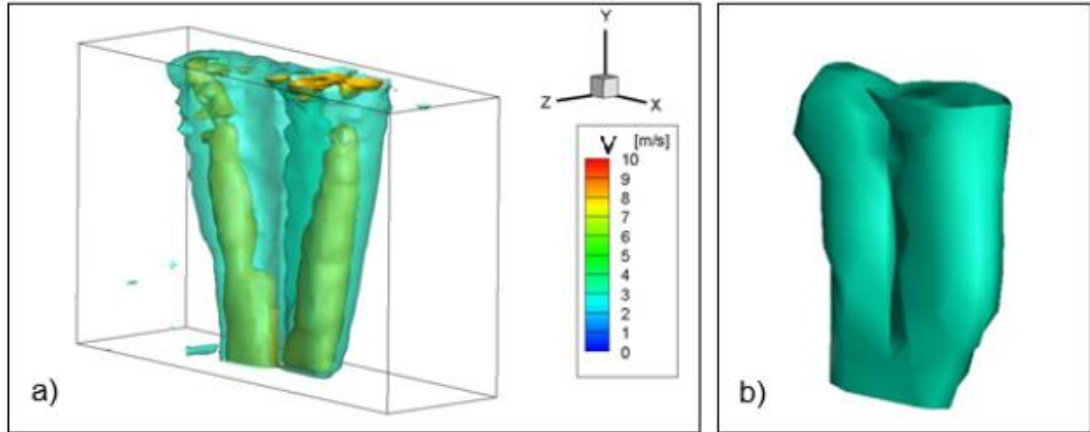


Figure 2.23 a) The three component volumetric average flow structure velocity surfaces, b) Volumetric flow structure obtained by three-dimensional background-oriented Schlieren method (Özer, Kuşluoğlu, & Yücekaya, 2017)

When Figure 2.23 is evaluated, it was observed that the core of the jet flow was divided into two from the mouth. This flow separation was similarly observed in the three-dimensional background-oriented Schlieren method results.

The quantitative knowledge is required for the ability to define data from experiments to the CFD program that is the main objective of this thesis. None of the density difference methods give quantitative data directly. For this reason, 3DBOS method, in which a jet flow was investigated, was not applied to outflow section of the air conditioner.

CHAPTER THREE

NUMERICAL STUDY

3.1 Computational Fluid Dynamics (CFD)

3.1.1 History of CFD

At the beginning of the 1970s, the history of the Computational Fluid Dynamics (CFD) started. Computers have been used for years because of the complex mathematics and physics used to solve flow problems. Many programs have been written for many years to solve these problems. The development of CFD continues in connection with the development of computer technologies. The beginning of CFD was triggered by more powerful computers. The method is still linked to the development of computer technologies. The first applications of the CFD methods was the simulation of transonic flows based on the solution of the non-linear potential equation. In the 1980s, the first two-dimensional and three-dimensional Euler equations were solved. With the mid 1980's, the focus started to shift to the significantly more demanding simulation of viscous flows governed by the Navier-Stokes equations. Together with this, a variety of turbulence models evolved with different degree of numerical complexity and accuracy. The leading edge in turbulence modelling is represented by the Direct Numerical Simulation (DNS) and the Large Eddy Simulation (LES). However, both approaches are still far away from being usable in engineering applications (Blazek, 2001).

With today's computer power, CFD has come to the capacity to solve much more complex problems in a very short time. As a result, CFD has become a method of analysis that saves time and money in many design processes.

3.1.2 The Mathematics of CFD

The continuity, momentum and energy equations, which are the basic equations of fluid dynamics, are the basis of CFD. They are the mathematical statements of three

fundamental physical principles upon which all of fluid dynamics is based on following conservation laws:

1. The conservation of mass,
2. The conservation of momentum,
3. The conservation of energy.

CFD applications have codes that use different solution methods. The most important ones are; Finite difference (FD), finite volume (FV) and finite element (FE) methods. The program used within the thesis uses the finite volume method. The investigation volume in this method is divided into sub-volumes and examined.

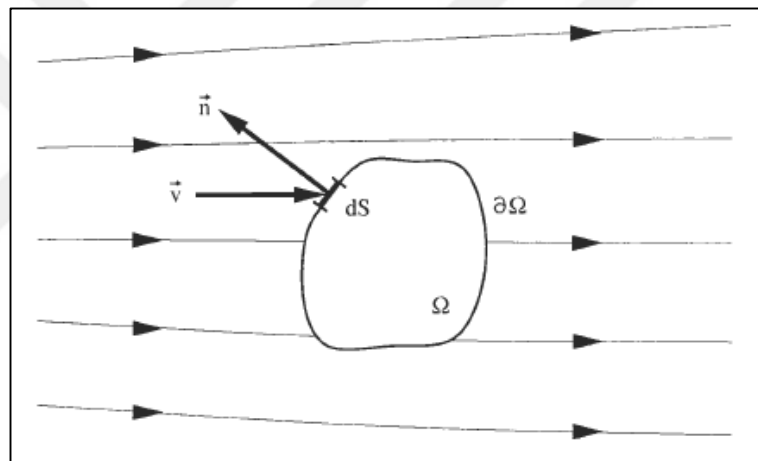


Figure 3.1 Definition of a control volume (fixed in space) (Blazek, 2001)

3.1.3 Conservation Laws

3.1.3.1 The Continuity Equation

The continuity equation can be derived using a finite control volume as shown in Figure 3.1. At a point on the control surface, the flow velocity is \vec{v} , the unit normal vector is \vec{n} and dS denotes an elemental surface area. . The conserved quantity in this case is the density ρ . For the time rate of change of the total mass inside the finite volume Ω , there is

$$\frac{\partial}{\partial t} \int_{\Omega} \rho d\Omega \quad (3.1)$$

The product of (density) x (surface area) x (velocity component perpendicular to the surface) is equal to the mass flow of a fluid through some surface. Therefore, the contribution from the convective flux across each surface element dS becomes

$$\rho = (\vec{v} \cdot \vec{n}) dS \quad (3.2)$$

\vec{n} always moves away from the control volume. If $(\vec{v} \cdot \vec{n})$ is negative, it can be defined as inflow, and if $(\vec{v} \cdot \vec{n})$ is positive, it can be defined as outflow.

$$\frac{\partial}{\partial t} \int_{\Omega} \rho d\Omega + \int_{\partial\Omega} \rho (\vec{v} \cdot \vec{n}) dS \quad (3.3)$$

Equation 3.3 represents the integral form of the continuity equation.

3.1.3.2 The Momentum Equation

Momentum equation can be derived from Newton's second law, which describes the momentum resulting from the net force acting on the mass element. For the momentum of control volume Ω

$$\rho \vec{v} d\Omega \quad (3.4)$$

The variation in time of momentum within the control volume equals

$$\frac{\partial}{\partial t} \int_{\Omega} \rho \vec{v} d\Omega \quad (3.5)$$

It can be said that the product of density times velocity is the conserved quantity.

$$\vec{\rho v} = [\rho u, \rho v, \rho w]^T \quad (3.6)$$

The coordinate system of the following components defines the convective flow tensor.

$$\text{x-component : } \rho u \vec{v}$$

$$\text{y-component : } \rho v \vec{v}$$

$$\text{z-component : } \rho w \vec{v}$$

The contribution of the convective flux tensor to the conservation of momentum is then given by

$$\oint_{\partial\Omega} \vec{\rho v} (\vec{v} \cdot \vec{n}) dS \quad (3.7)$$

Two types of force acting on the control volume can be mentioned. The first of these are the external volume or body forces that influence the mass of volume. Examples of these are gravity, buoyancy etc. The other is the surface forces acting directly from the surface of the control volume. These surface forces can be the pressure distribution applied by the external flow or the shear or normal stresses caused by friction.

The contribution of the body (external) force to the momentum conservation is

$$\int_{\Omega} \rho \vec{f}_e d\Omega \quad (3.8)$$

Isotropic pressure and viscous stress $\vec{\tau}$ tensor composes surface sources.

$$\vec{Q}_s = -p\vec{I} + \vec{\tau} \quad (3.9)$$

In Figure 3.2, the surface sources are shown.

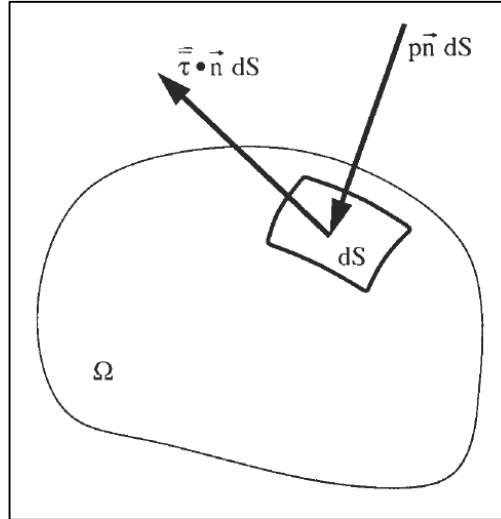


Figure 3.2 Surface forces acting on a surface element of the control volume (Blazek, 2001)

The following expression (Equation 3.10) is obtained when all the above equations are taken into consideration.

$$\frac{\partial}{\partial t} \int_{\Omega} \rho \vec{v} d\Omega + \oint_{\partial\Omega} \rho \vec{v} (\vec{v} \cdot \vec{n}) dS = \int_{\Omega} \rho \vec{f}_e d\Omega - \oint_{\partial\Omega} p \vec{n} dS + \oint_{\partial\Omega} (\vec{\tau} \vec{n}) dS \quad (3.10)$$

Equation 3.10 expresses momentum conservation in a control volume.

3.1.3.3 The Energy Equation

The energy equation can be derived using the first law of thermodynamics. The net heat flux in the volume and the rate of work of forces cause changes in time of the total energy inside the volume. The total energy per unit mass can be found by adding the internal energy per unit mass of the kinetic energy per unit mass. Total energy can be written as follows.

$$E = e + \frac{|\vec{v}|^2}{2} + \frac{u^2 + v^2 + w^2}{2} \quad (3.11)$$

The conserved equation is the total energy per unit volume. The total energy variation in time is

$$\frac{\partial}{\partial t} \int_{\Omega} \rho E d\Omega \quad (3.12)$$

The contribution of the convective flow can be expressed as

$$\oint_{\partial\Omega} \rho E (\vec{v} \cdot \vec{n}) dS \quad (3.13)$$

The diffusive flux which does not exist in continuity and momentum equations exists in energy equation. Only internal energy is influential because of the diffusive flux \vec{F}_D is defined for fluid at rest.

$$\vec{F}_D = -\gamma \rho \kappa \nabla e \quad (3.14)$$

In Equation 3.14, $\gamma = \frac{c_p}{c_v}$ is the specific heat coefficient and κ is the thermal diffusivity coefficient. Equation 3.14 can be expressed as the Fourier law of heat conduction. In Equation 3.15, k represents the thermal conductivity coefficient and T represents the absolute static temperature.

$$\vec{F}_D = -k \nabla T \quad (3.15)$$

Volumetric heating due to chemical reactions or due to radiation is another part of the net heat flux entering the finite control volume. We will denote the heat sources - the time rate of heat transfer per unit mass - as \dot{q}_h . Together with the rate of work done by the body forces \vec{f} , which we have introduced for the momentum equation, it completes the volume sources;

$$Q_v = \rho \vec{f} \cdot \vec{v} + \dot{q}_h \quad (3.16)$$

The last parameter affecting the conservation of the energy is surface sources \vec{Q}_s . They correspond to the time rate of work done by the pressure as well as the shear and normal stresses on the fluid element;

$$\vec{Q}_s = -p\vec{v} + \vec{\tau}\vec{v} \quad (3.17)$$

The conservation of energy (Equations 3.17) can be expressed using the above equations.

$$\frac{\partial}{\partial t} \int_{\Omega} \rho E d\Omega + \oint_{\partial\Omega} \rho E (\vec{v}\vec{n}) dS = \oint_{\partial\Omega} k (\nabla T \vec{n}) dS + \int_{\Omega} (\rho \vec{f}_e \vec{v} + \dot{q}_h) d\Omega - \oint_{\partial\Omega} p (\vec{v}\vec{n}) dS + \oint_{\partial\Omega} (\vec{\tau}\vec{v}) \vec{n} dS \quad (3.18)$$

3.2 Numerical Study

In this study, the three-dimensional velocity and temperature distributions obtained by the experimental methods described in Section 2.1.1 and Section 2.1.2 are used as input in the numerical model using the Computational Fluid Dynamics (CFD) method. Thus, the input conditions used in the CFD analyzes were supported by experimental data, and the velocity and temperature distributions of the conditioned air in different room geometries were examined.

For this study, a Computer Aided Design (CAD) model was taken from a company that produces split air conditioner indoor units. The CAD model is shown in Figure 3.3 and Figure 3.4.

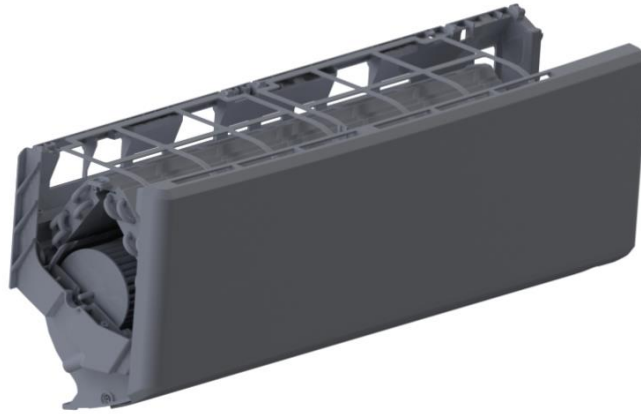


Figure 3.3 Isometric view of the CAD model of split air conditioner indoor unit

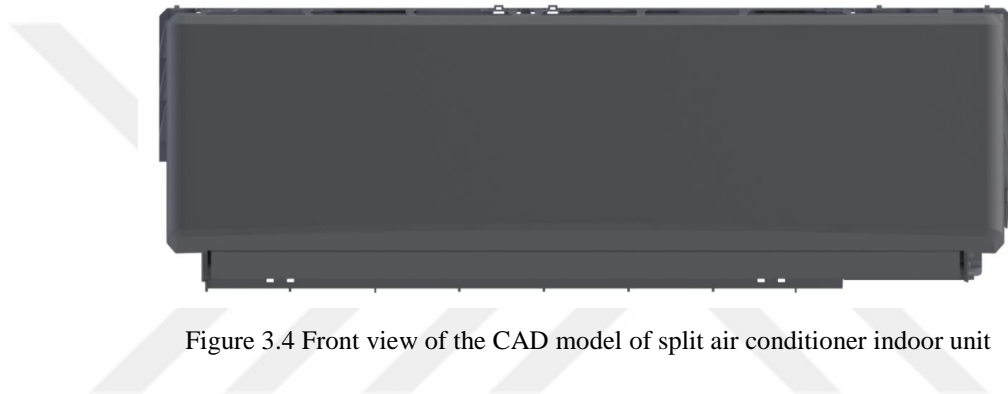


Figure 3.4 Front view of the CAD model of split air conditioner indoor unit

3.2.1 CFD Model

In order to obtain the flow and temperature distribution in the room, the split air conditioner indoor unit CAD model was placed in the room geometry. Room geometry was modeled as air volume. The volume of the air conditioner was subtracted from the air volume and the surfaces of the outflow and suction section of the air conditioner were formed.

The room geometry was modeled to change parametrically, as the effects of the outflow section on different room geometries were investigated. The air volume of the three-dimensional room model and the location of the air conditioner in the model are shown in Figure 3.5.

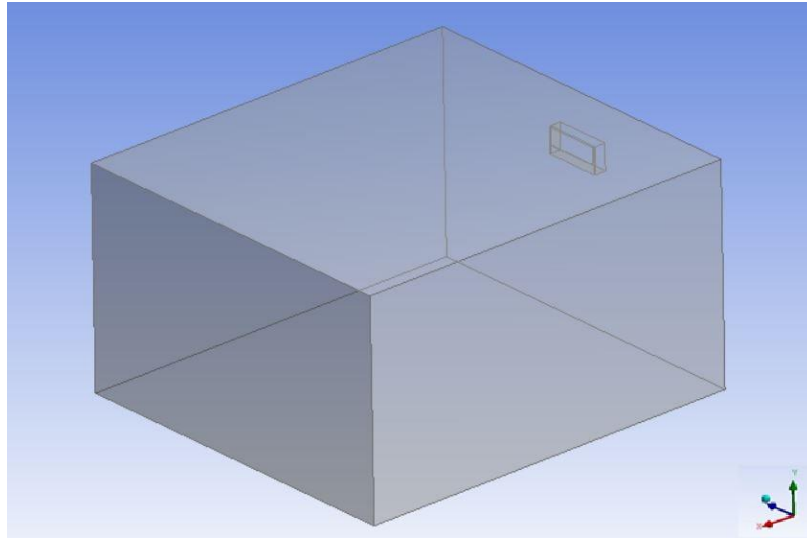


Figure 3.5 The air volume of the three-dimensional room model

3.2.2 Meshing

Meshing has an important place in CFD analysis. The number of elements, elements quality etc. can directly influence the results of analysis. In addition, meshing affects key elements for analysis such as CPU time and convergence of analysis.

In the study, a commercial CFD analysis program was used to construct the mesh structures. There are many different mesh elements available in the program. Tetrahedral elements which are widely preferred and which give better results especially on curved surfaces were preferred in the current study. The mesh structure of the numerical model of room air volume mentioned in Section 3.2.1 is shown in Figure 3.6.

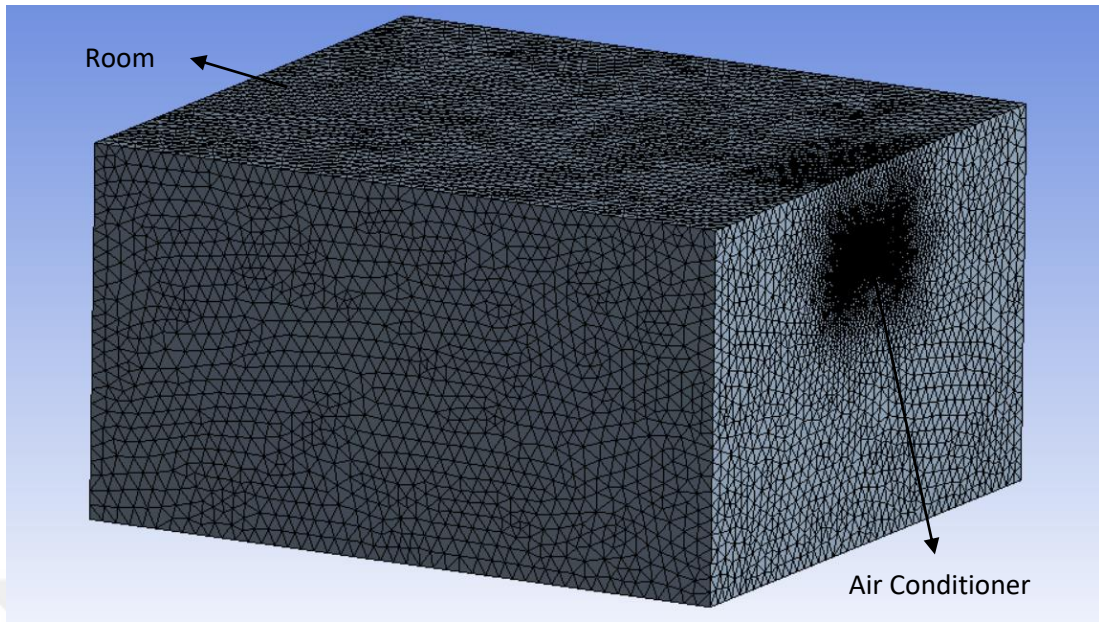


Figure 3.6 Mesh structure of numerical model

The air conditioning outflow and suction sections defined by the boundary conditions meshed with a high number of elements. Thus, it was aimed to obtain more precise results. In addition, more data was obtained by the higher number of elements in the boundary conditions, thus approaching the number of data obtained by the experimental work. The elements of boundary conditions are shown in Figure 3.7.

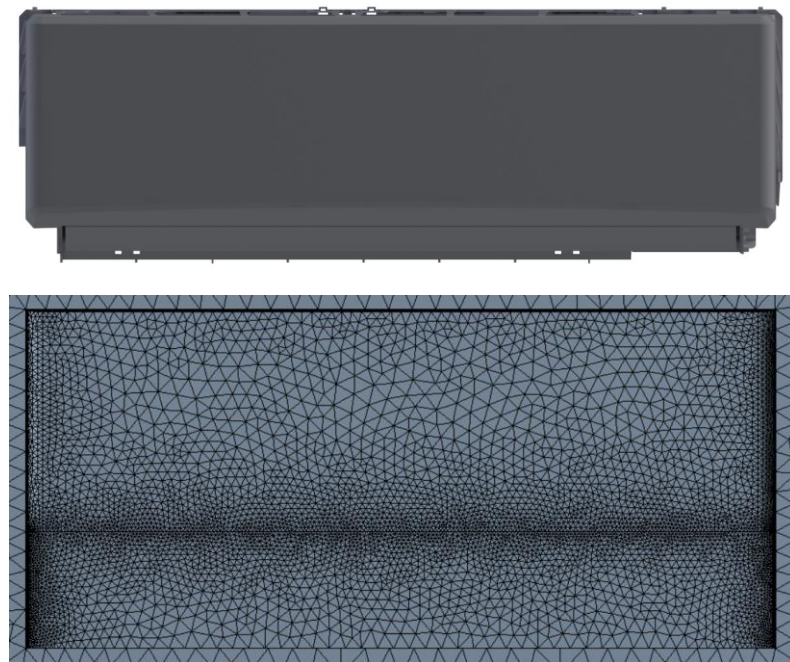


Figure 3.7 Mesh structure of split air conditioner indoor unit

Models with different element numbers were analyzed while forming the mesh structure of the numerical model. The reason for this is the mesh independence study. By doing the mesh independence study, the analysis time and CPU power have been saved. In this context, 6 different analyses, each with different element numbers, were performed. The characteristics of these 6 different analysis are given in Table 3.1.

Table 3.1 Details of mesh independence study

Number of Elements	Element Quality	Duration of Analysis (min)
284169	0.83136	11
630991	0.84705	27
798983	0.84432	33
1096936	0.8476	48
1550478	0.85029	67
2194314	0.85159	98

In the process of mesh independence study, velocity and temperature data were taken from a point in the jet fluid near the outflow section of split air-conditioner indoor unit. In addition, average velocity and average temperature data were obtained from a plane in the middle of the room. The position of the point and the position of the middle plane where the data were taken are shown in Figure 3.8.

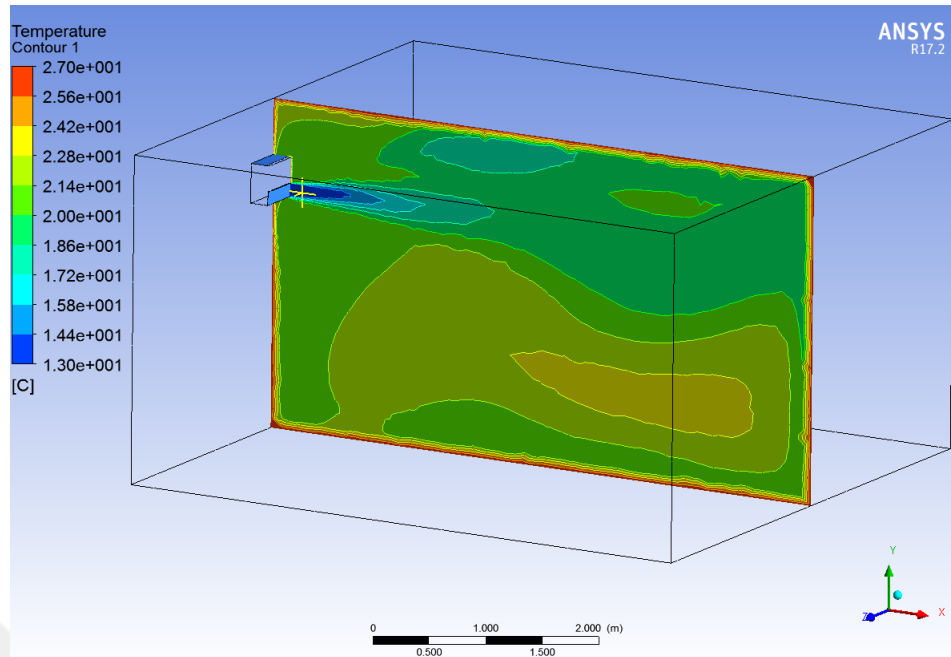


Figure 3.8 The position of the data point and plane

The number of elements that these values negligibly changed was chosen as the appropriate mesh structure for the analysis. This value is 1096936 as can be seen in the graphic given in Figure 3.9.

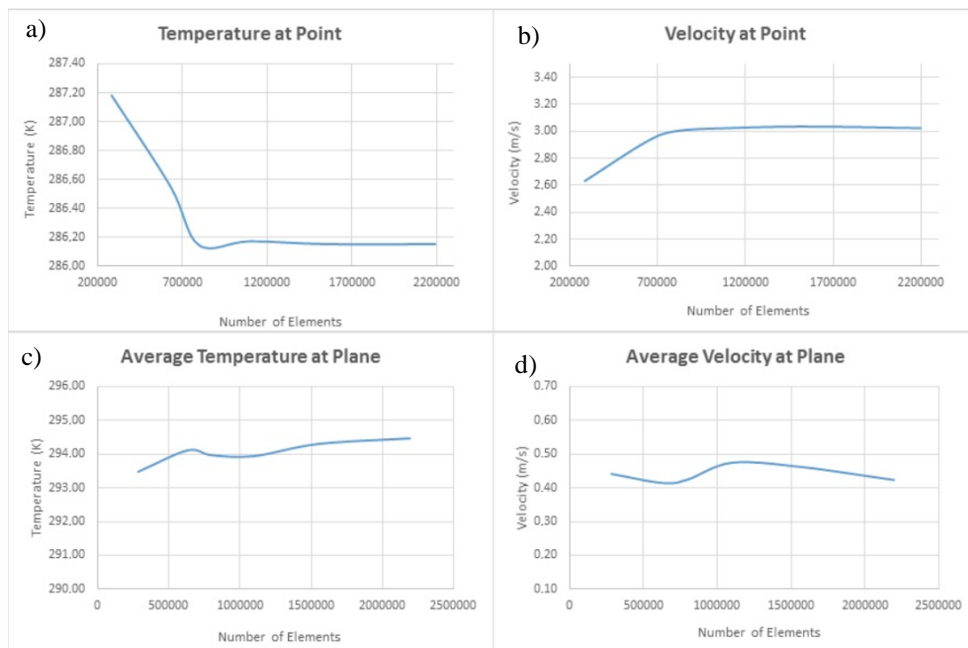


Figure 3.9 a) Temperature values at point for different number of elements, b) Velocity values at point for different number of elements, c) Average temperature values at plane for different number of elements, d) Average velocity values at plane for different number of elements

As can be seen from the graphs in Figure 3.9, there is no significant change in the number of elements above from 1096936 elements. For this reason, the number of 1096936 elements was chosen as the final model.

An iteration independence study was done for the selected number of elements. When the analysis results were examined, it was seen that the required residual values were reached after about 300 iterations. But the effects of the results were examined by testing different iteration numbers. Details of this study are given in Table 3.2.

Table 3.2 Details of iterations independence study

Number of Iterations	Duration of Analysis (min)
500	48
1000	96
1500	141
2000	191
5000	454

As in the mesh independence study, velocity and temperature data were taken from a point in the jet fluid near the outflow section of split air-conditioner indoor unit. In addition, average velocity and average temperature data were obtained from a plane in the middle of the room. The velocity and temperature values for the plane and the point are given in Figure 3.10.

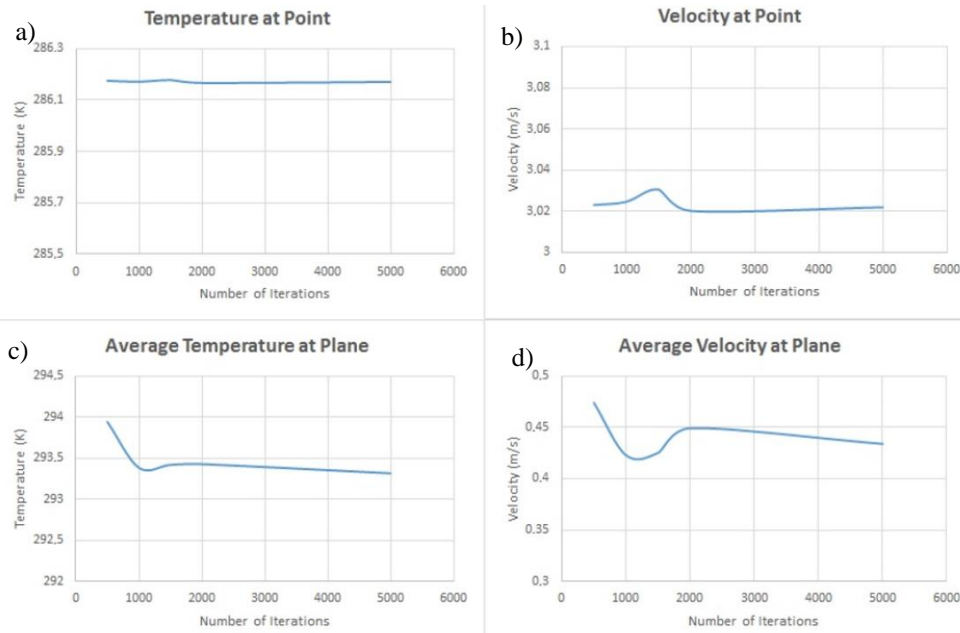


Figure 3.10 a) Temperature values at point for different number of iterations, b) Velocity values at point for different number of iterations, c) Average temperature values at plane for different number of iterations, d) Average velocity values at plane for different number of iterations

As can be seen from Figure 3.10, the difference between the numbers of iterations did not make any significant change in the results. For this reason, 500 iterations were selected for analysis.

3.2.3 Boundary Conditions

The boundary conditions of the room air volume described in Section 3.2.1 was defined in the CFD program. In the analysis, the behavior of the air in the room has been investigated by defining both the velocity and the temperature of the outflow section of the air conditioner indoor unit.

The walls of the room were defined at a homogenous temperature of 27°C . Furthermore, the air in the room was chosen as ideal gas. The upper side of the air conditioner which is suction section was defined as the outlet boundary condition and the relative pressure was entered 0 Pa as outlet conditions.

The boundary conditions of the outflow section of the air conditioner was defined by the method developed in the current study. In this method, the velocity vectors obtained from the PIV experiments described in section 2.1.1 and the temperature data obtained from the MIT experiments described in section 2.1.2 were defined as input conditions in the CFD program.

A code has been developed to define to the outflow section of the air conditioner the velocity and temperature values obtained from experiments. In the developed code, the velocity and temperature values obtained from the experiments form a matrix together with the position information. The location information in this matrix were compared with the location information from the CFD program. The experimental data from the PIV and MIT methods and the data exported from the CFD were compared using the nearest neighbor algorithm. According to the logic of this algorithm, the experimental data having the position closest to the position information in the CFD was selected and a new matrix is created to use the CFD position information and the velocity and temperature information on the experimental data. Using the nearest neighbor algorithm is disadvantageous when there is more distance between the two data to match. However, the number of data in the PIV method which was used to obtain velocity data was about 55 times greater than the number of data exported from CFD. For this reason, the error of finding the nearest neighbors is negligible. When creating temperature data to be entered into the CFD program as a boundary condition, the advantage of using this algorithm is that there was not much difference between the temperature values.

As a result of the comparison, positions that were close to each other below a certain error rate were matched and a new matrix was created to enter the CFD program. Thus, the velocity and temperature data obtained from experiments, which have a separate value for each position, were defined at outflow section of the air conditioner in the CFD program.

In the literature, homogeneous velocity and temperature profiles are defined in the outflow section of the air conditioner. With the developed method, unlike the

literature, the actual velocity and temperature profiles obtained from the experiments are defined in the outflow section of the air conditioner. Thus, the actual state of the air conditioner is given as a model input, and the flow structure and temperature distribution of the outflow section of the air conditioner are modeled closer to reality.

3.2.4 Solver

As mentioned in section 3.2.2, the number of meshes chosen approximately 1 million and the number of iterations chosen 500 for the numerical model. After the definitions of boundary conditions (material types, domain motion, temperature, pressure, heat transfer mechanisms, turbulence models etc.) and initial conditions, solver control definitions were made. To simulate the characteristics of turbulent flow, the standard $k-\varepsilon$ turbulence model was used because of its wide capability. The heat transfer, momentum, mass and turbulence residuals of three-dimensional steady-state analyses that were formed separately in four different analyses are shown in Figure 3.11, Figure 3.12 and Figure 3.13.

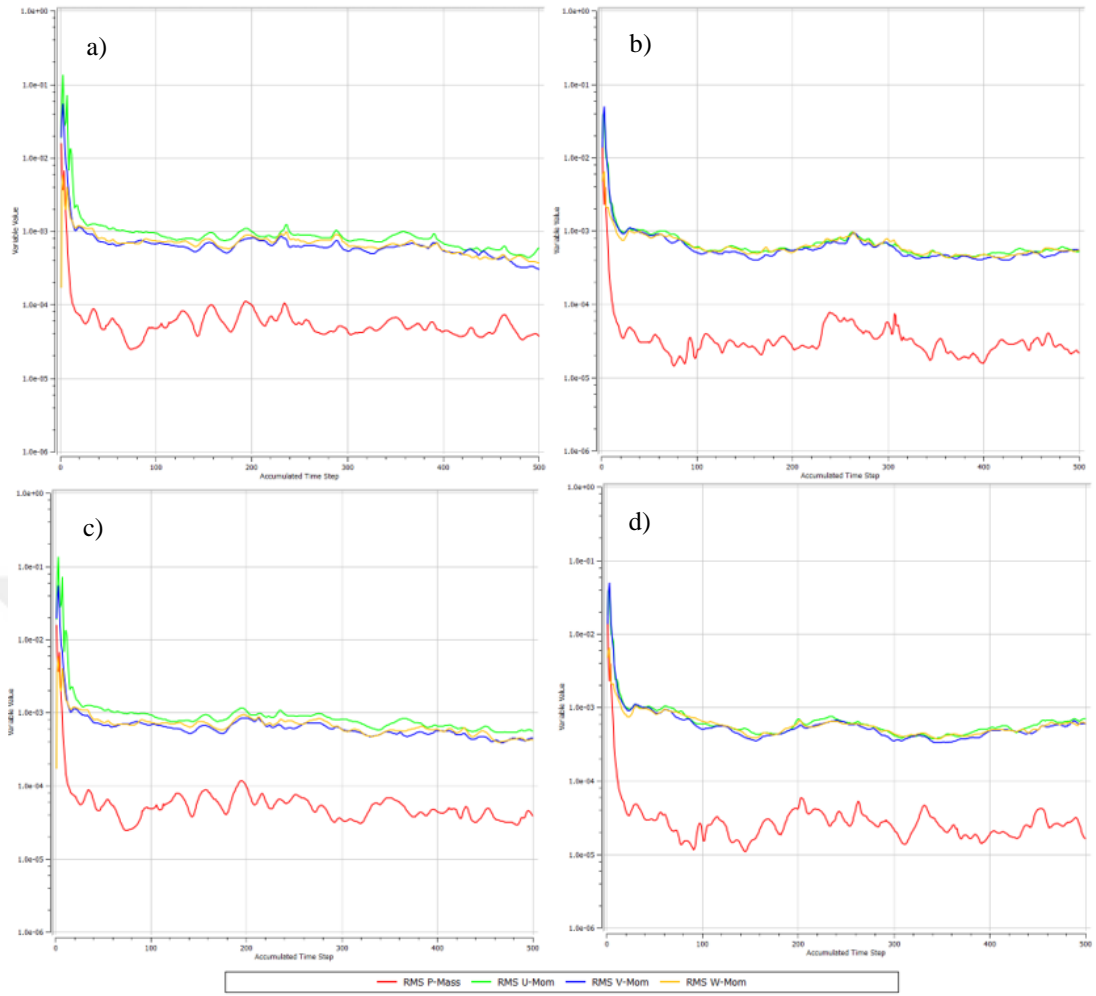


Figure 3.11 Momentum and mass residuals of analyses a) temperature: homogeneous, velocity: homogeneous, b) temperature: homogeneous, velocity: PIV, c) temperature: MIT, velocity: homogeneous, d) temperature: MIT, velocity: PIV

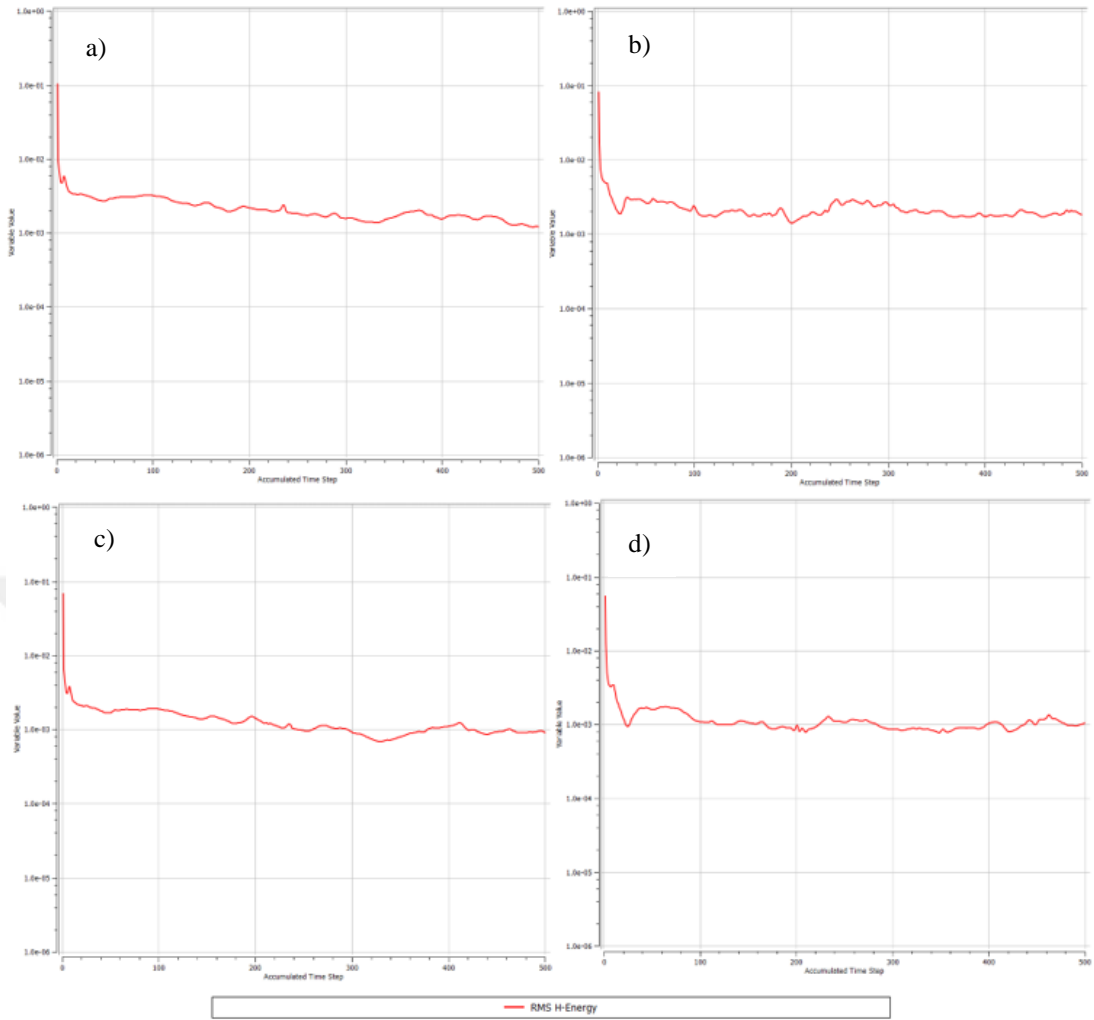


Figure 3.12 Heat transfer residuals of analyses a) temperature: homogeneous, velocity: homogeneous, b) temperature: homogeneous, velocity: PIV, c) temperature: MIT, velocity: homogeneous, d) temperature: MIT, velocity: PIV

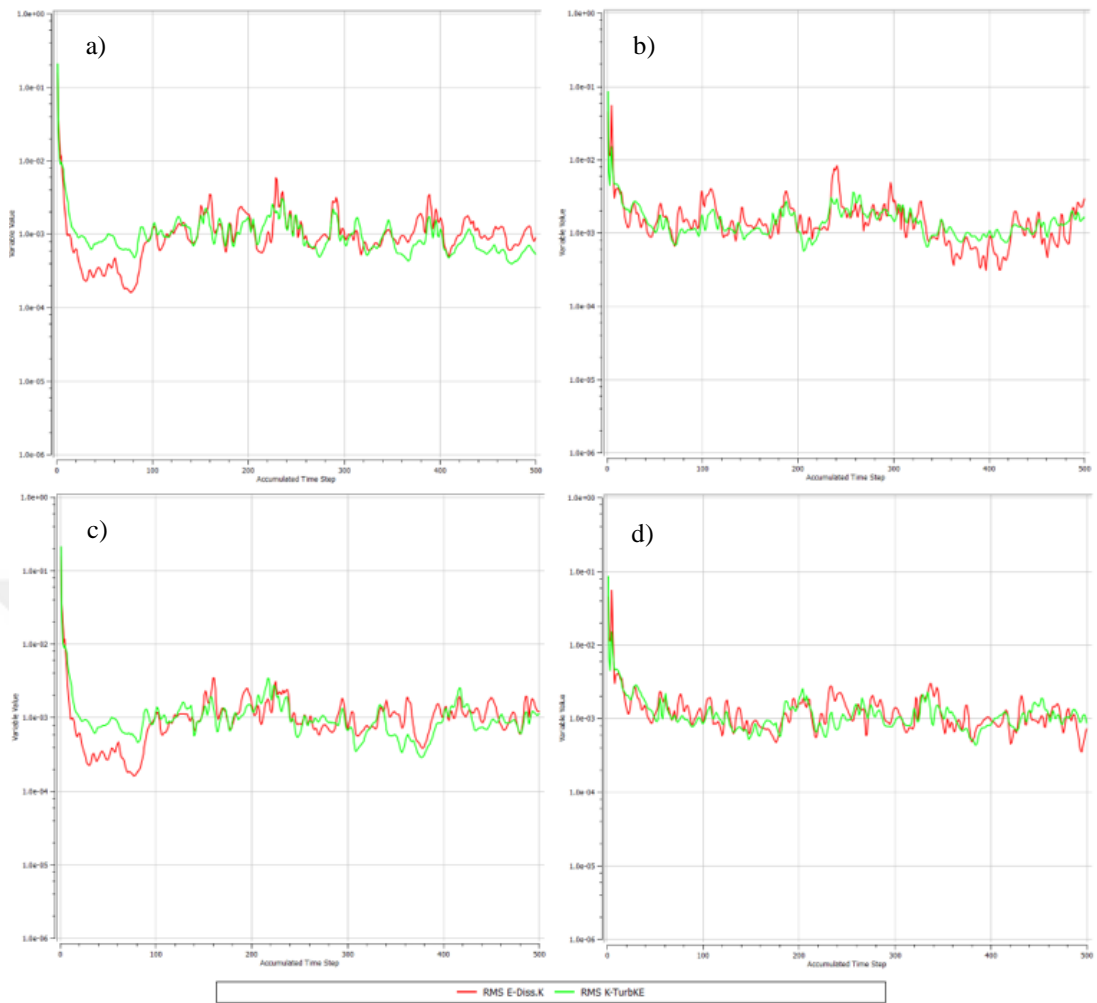


Figure 3.13 Turbulence residuals of analyses a) temperature: homogeneous, velocity: homogeneous, b) temperature: homogeneous, velocity: PIV, c) temperature: MIT, velocity: homogeneous, d) temperature: MIT, velocity: PIV

CHAPTER FOUR

RESULTS AND DISCUSSIONS

Despite the fact that numerous studies which theoretical, experimental and numerical methods are applied separately are in the literature, the number of studies in which these methods are used together is limited. In conventional CFD studies, only the average velocity and temperature values of the experimental results are used for boundary conditions. This means that the value defined as the input is averaged in terms of location and value. Therefore, velocity defined as normal to outflow section. In the literature, every value of velocity and temperature in the outflow section of the air conditioner is considered equal. This means that the information defined in the outflow section is one-dimensional in these CFD studies which are not able to define vector components of velocity at each point.

In this study, unlike the literature, three-dimensional velocity and temperature data obtained from the experiments were defined as boundary conditions. In our study, the three-dimensional and three-component velocity data obtained from the PIV experiment allowed defining vector components of velocity in CFD program. Thereby, both local and volumetric effects in the defined regions were defined as boundary conditions. Which allowed the airflow in the room to be modeled closer to reality than only using CFD methods. For comparison, additional analyses have been done. In this analyses, for simulating the conventional studies, the average values used. These values also extracted from PIV and MIT data.

The boundary conditions given as inputs to the outflow section of the split air conditioner indoor unit were examined with different definitions in 4 different analyses and the effects of parameters such as velocity, temperature were investigated to each other and to the flow structure.

In the first of the analyses, the average velocity and temperature values obtained from the PIV and MIT experiments were defined as a homogeneous velocity and a homogeneous temperature boundary conditions (Figure 4.1-a). In the second analysis,

the velocity values obtained from the PIV experiment were defined as the boundary condition to the outflow section. The average value of the data obtained from the MIT experiment was used as a homogenous temperature input of outflow section in this analysis (Figure 4.1-b). In the third analysis, the temperature values obtained from the MIT experiment were defined as the boundary condition to the outflow section. The average of the velocity values obtained from the PIV experiment was used as a homogenous velocity for the analysis (Figure 4.1-c). In the fourth analysis, the values from the MIT and PIV experiments were defined as the velocity and temperature input to the outflow section (Figure 4.1-d). The homogeneous velocity obtained by averaging PIV experiment data is 2.55 m/s (Figure 4.1-a and c). The homogeneous temperature obtained by averaging MIT experiment data is 294.39 K (Figure 4.1-a and b).

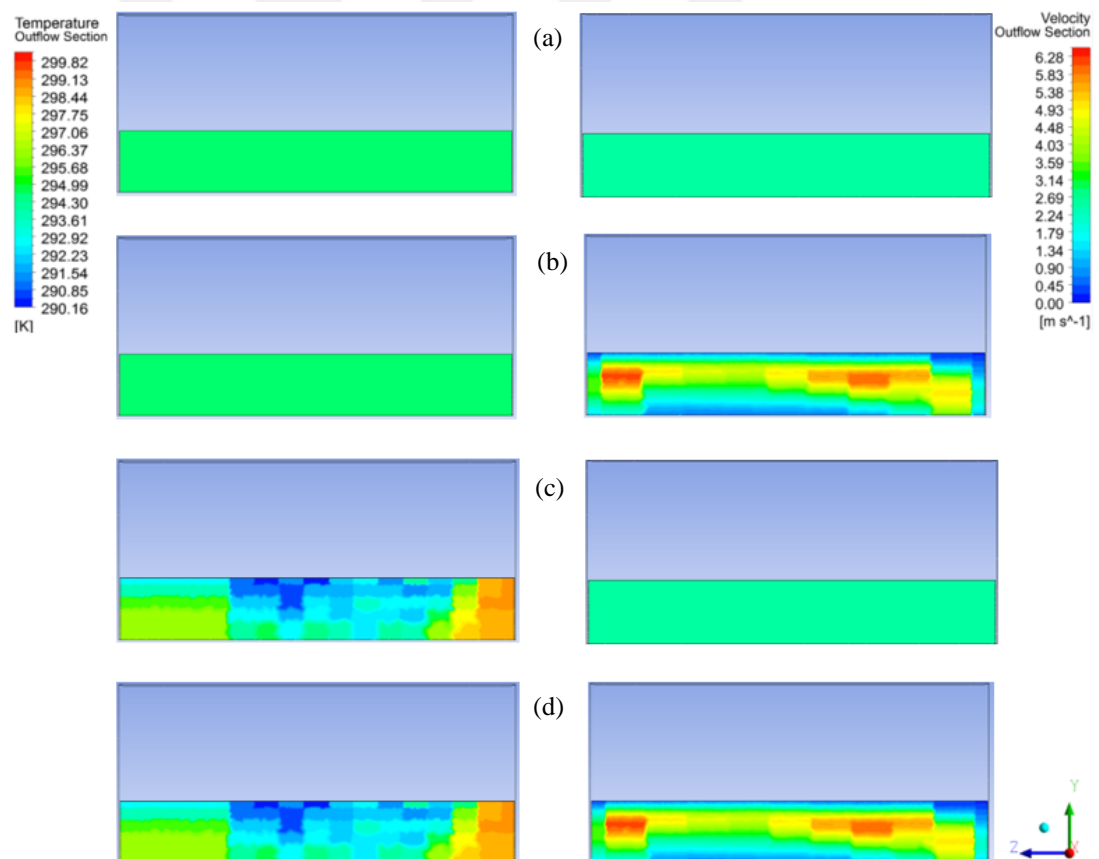


Figure 4.1 Boundary conditions of outflow section: a) temperature: homogeneous, velocity: homogeneous, b) temperature: homogeneous, velocity: PIV, c) temperature: MIT, velocity: homogeneous, d) temperature: MIT, velocity: PIV

When a homogeneous velocity was defined at the outflow section of the indoor unit (Figure 4.1-a and 4.1-b), a very different velocity distributions was observed from the actual velocity profile. The outflow section velocity defined by the PIV experiment was compared with the outflow section with a homogeneous velocity value defined. Defining a homogeneous value in the outflow section is wrong in terms of the both flow profile and the size of the flow. The fact that the data obtained from PIV experiments are defined as boundary condition removes these disadvantages. In addition, another advantage of defining PIV experiments as boundary conditions is to define three-dimensional effects of flow. This provides vectorial correctness in velocity definition.

The outflow section velocity distribution is a double-heads velocity profile due to the blowing characteristic of the cross flow fan (CFF) which is located in the air conditioner indoor unit. This situation, which is described in the literature, is caused by the presence of secondary flows under the jet flow (Karadeniz, Kumlutaş, & Özer, 2013). These flows move towards each other in the opposite direction. Flows that meet in the regions close to the jet center will blow up the jet. Thus a double-heads velocity profile occurs. The volumetric velocity profile of outflow section of air conditioner indoor unit obtained from PIV experiments is shown in Figure 4.2.

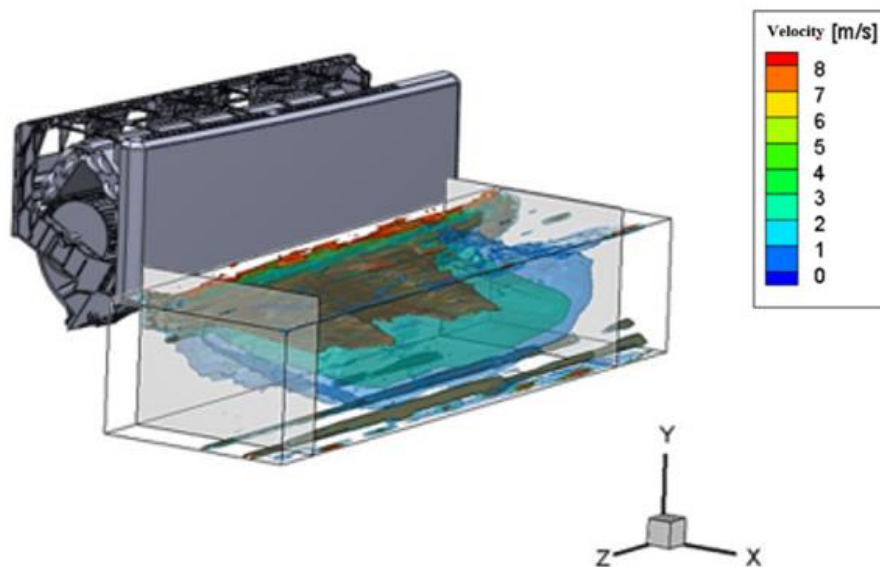


Figure 4.2 Average volumetric velocity profile at the outflow section of the split air conditioner

Figure 4.2 shows that defining a homogenous velocity value as a boundary condition is not true in every location of the outflow section. This affects many parameters such as jet penetration, temperature distribution and flow structure in the room. The penetration of the jet flow, which is one of the critical parameters when the indoor climates are examined, is different between the analysis a and the analysis b in Figure 4.3.

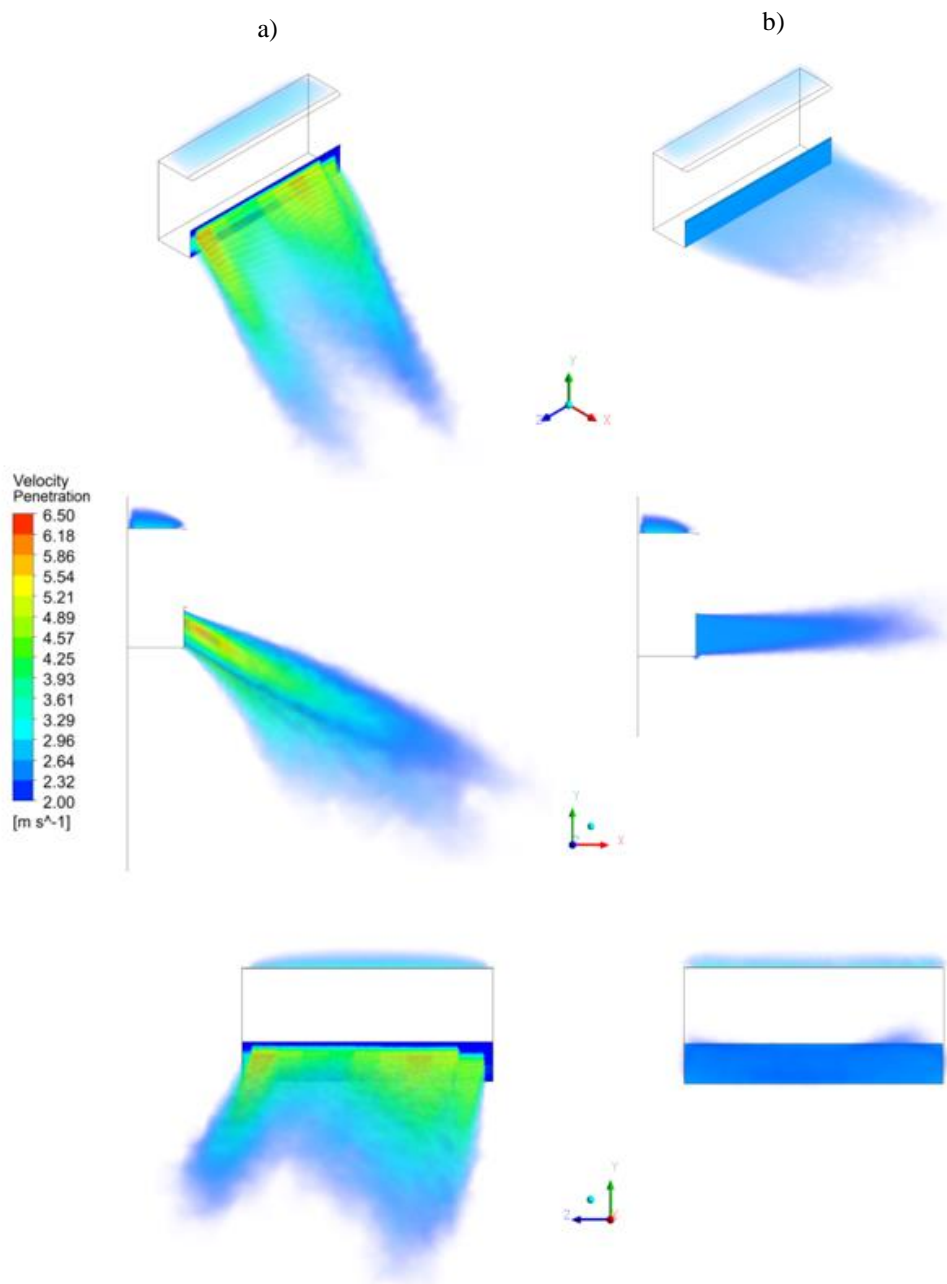


Figure 4.3 Penetration of outflow section of air conditioner indoor unit, a) Temperature: MIT, velocity: PIV, b) Temperature: MIT, velocity: homogeneous

Visualization of air flow velocity in the XY mid plane of the room is presented in Figure 4.4. In Figure 4.4, a is the analysis of the PIV data as the velocity input and b is the analysis of the homogeneous velocity value input as the velocity input.

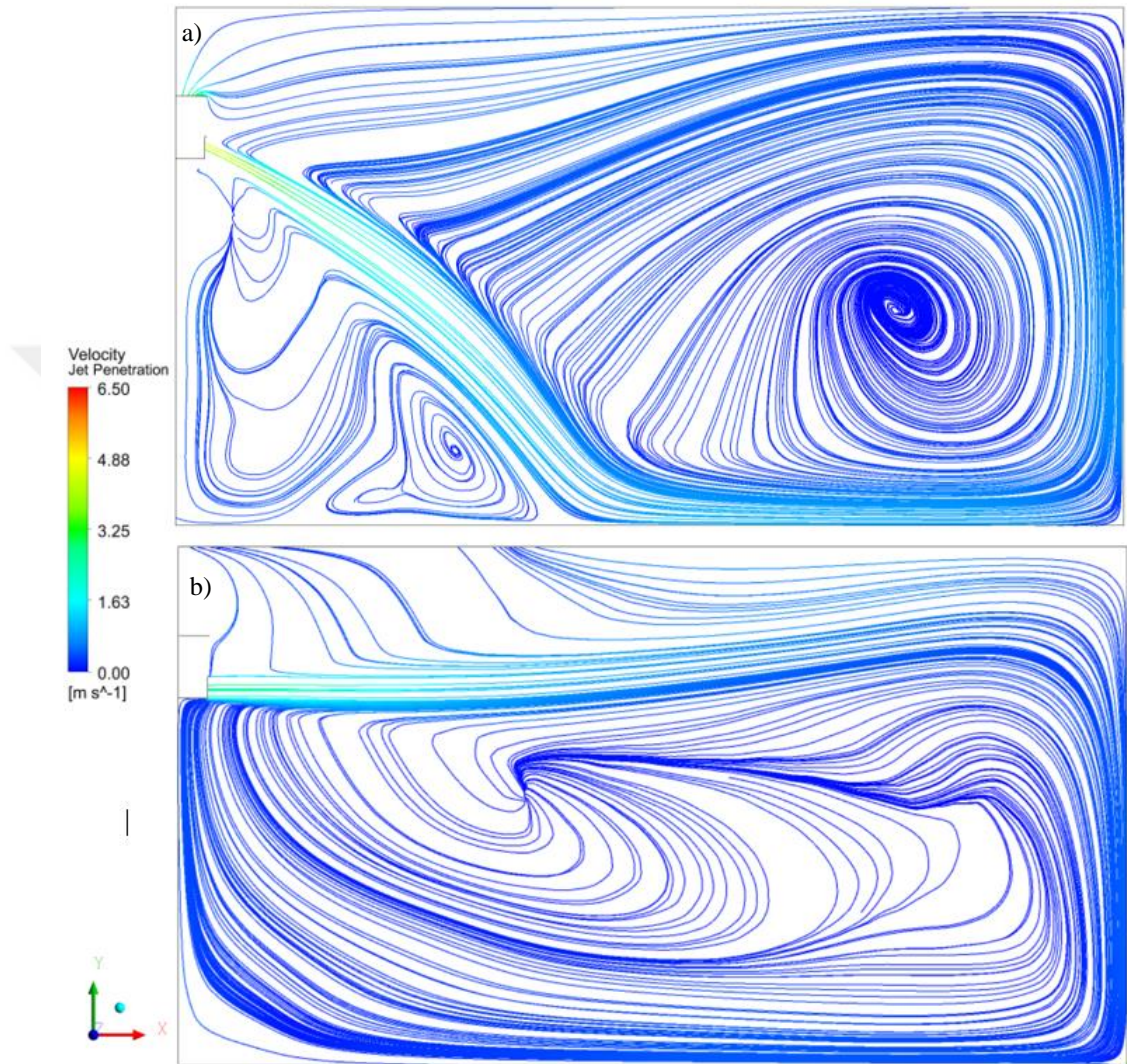


Figure 4.4 Streamline visualization of mid plane of room: a) Temperature: homogeneous, velocity: PIV
 b) Temperature: homogeneous, velocity: homogeneous

In the b analysis, it began to lose the jet effect at a shorter distance than the a analysis. Therefore, the amount of air diffusing of the conditioned air into the room also differed between the two analyses. In the a analysis, the penetration of the jet flow appears to be higher than the b analysis, since the data obtained from the PIV along the surface were defined in the boundary condition. Another important parameter seen in Figure 4.4 is the direction of flow. The horizontal directing airfoil, which does not

appear in the analysis, but actually exists, directs the fluid and distributes it more easily in the room. This is seen in Figure 4.4-a which the experimental data is given as a boundary condition.

When the above plane of 1.70 m, which is the height of the average human height, was examined from the ground, the difference of the flow distributions between the two different analyses was remarkable. The flow distributions in these planes are shown in Figure 4.5.

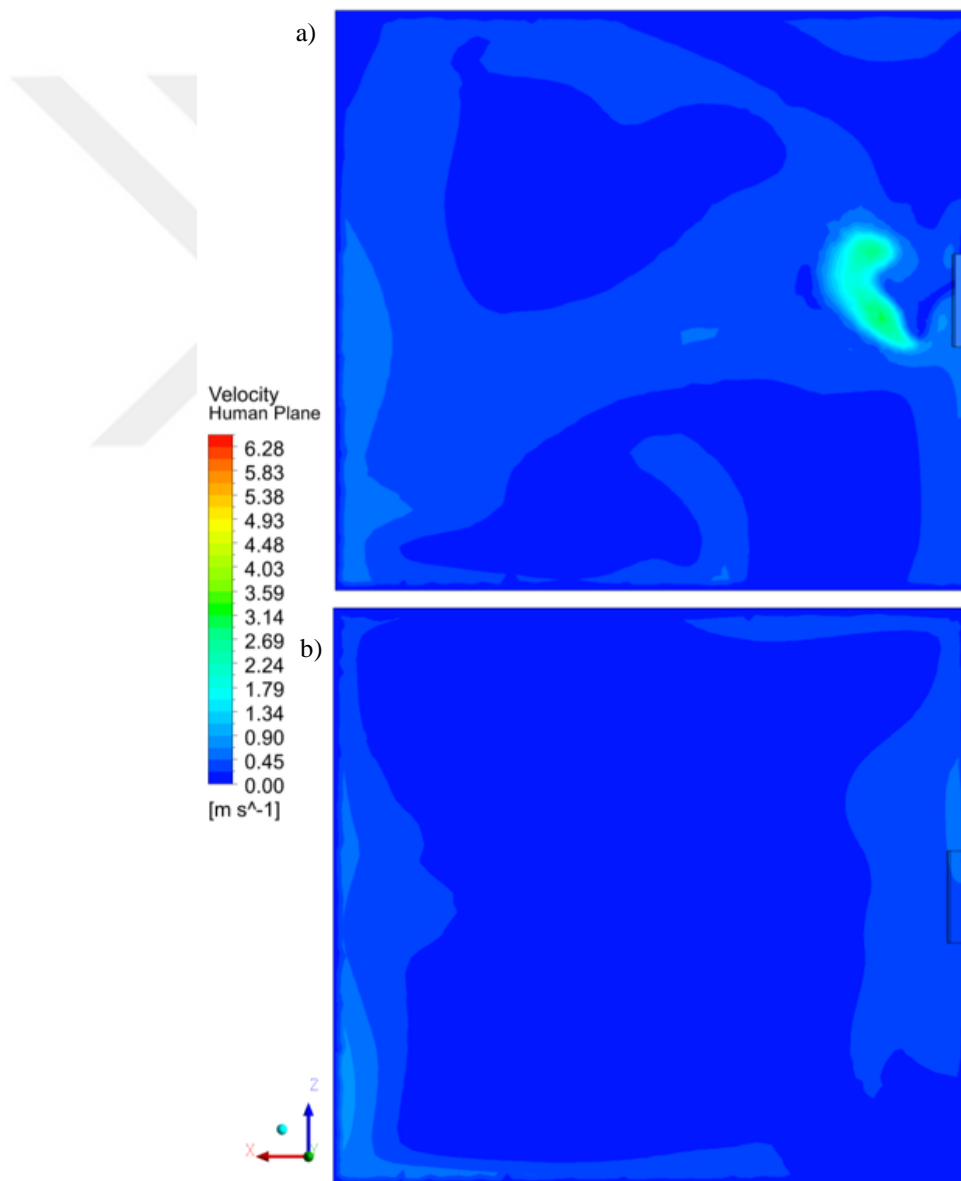


Figure 4.5 Velocity distributions at 1.70 m above ground of room: a) Temperature: homogeneous, velocity: PIV, b) Temperature: homogeneous, velocity: homogeneous

As seen in Figure 4.5-a, the corresponding part of the airflow blowing has taken the form due to the double headed flow structure mentioned in Figure 4.2. Besides, as shown in Figure 4.5, the definition of the PIV data at the outflow section affects the flow velocity in the room and hence the heat transfer with convection. This effect can be seen in Figure 4.6.

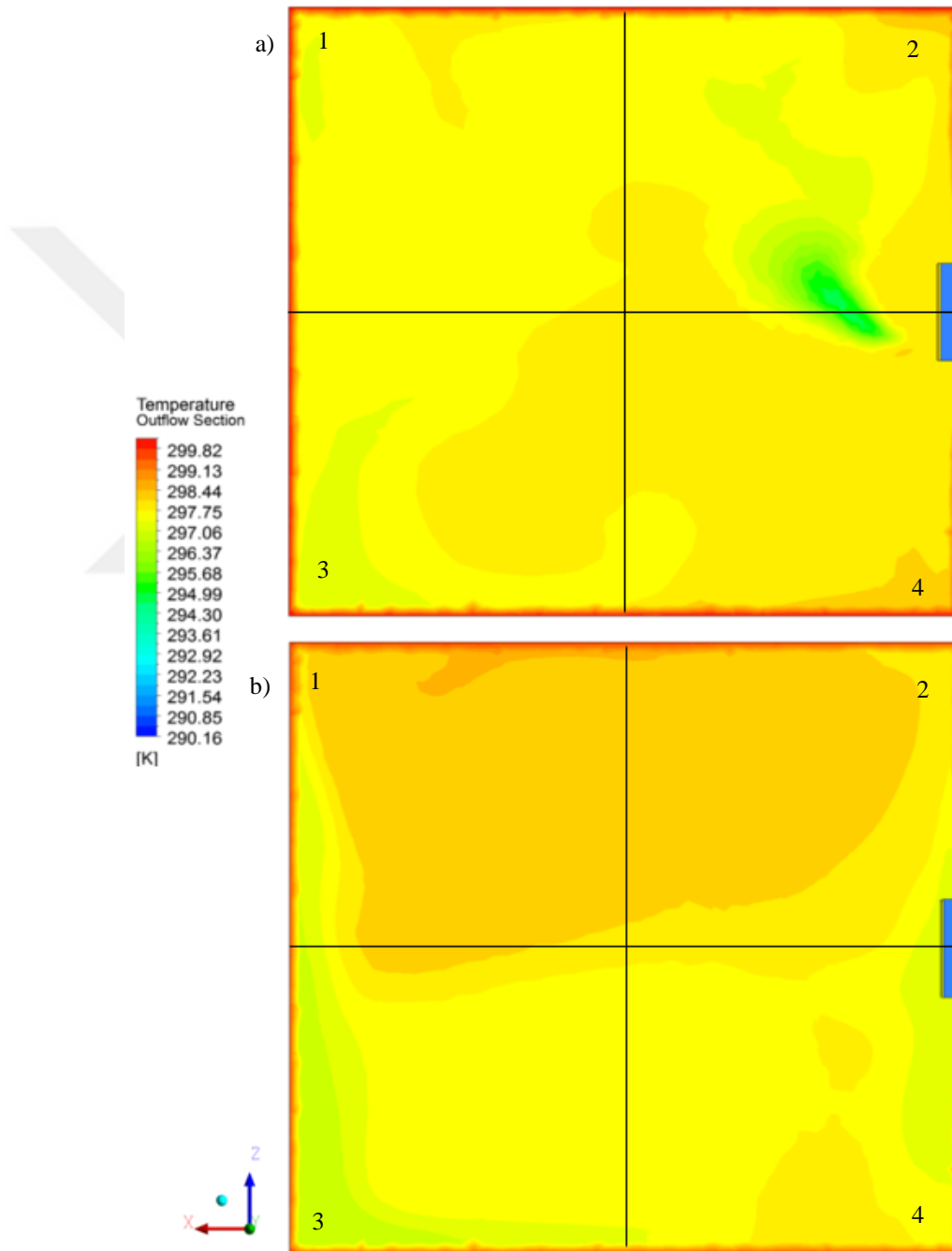


Figure 4.6 Temperature distributions at 1.70 m above ground of room: a) Temperature: MIT, velocity: PIV, b) Temperature: MIT, velocity: homogeneous

In Figure 4.6, 2 analyses which has the same boundary conditions obtained from MIT and the different velocity definitions were compared. The a and b analyzes in Figure 4.6 were divided into 4 regions and average temperature values in these regions were obtained. These values are presented in Table 4.1.

Table 4.1 The temperature values of the regions in Figure 4.6

Analysis	Region 1	Region 2	Region 3	Region 4
a	297.621 K	297.535 K	297.647 K	297.808 K
b	298.496 K	298.410 K	297.836 K	297.959 K

As can be seen in Figure 4.6, the definition homogeneous velocity data as the boundary condition causes the outflow section of the air conditioner to behave like air curtain in the flow structure and therefore in temperature distribution. In Figure 4.6-b, it can be seen that the temperature distribution of the room is divided into two. Besides, as seen in Table 4.1, especially when comparing the first and second regions, the temperature differences between the a and b analyzes are remarkable.

The effect of the boundary condition defined of the temperature data obtained by MIT method on the analyses is shown in Figure 4.7. The analysis a in Figure 4.7 represents the temperature distribution from the plane of human height in the analysis in which the temperatures obtained from the MIT method were defined. The difference in temperature distribution between the a analysis and the b analysis in which a homogeneous temperature value was defined showed that defining the experimental data as the boundary conditions are of importance to the modeling of the temperature distributions. The a and b analyzes in Figure 4.7 were divided into 4 regions and average temperature values in these regions were obtained. These values are presented in Table 4.2.

When Figure 4.7 and Table 4.2 are examined, define the experimental data as a boundary condition are different from defining the homogeneous data as a boundary condition in regards of both temperature value and temperature distribution.

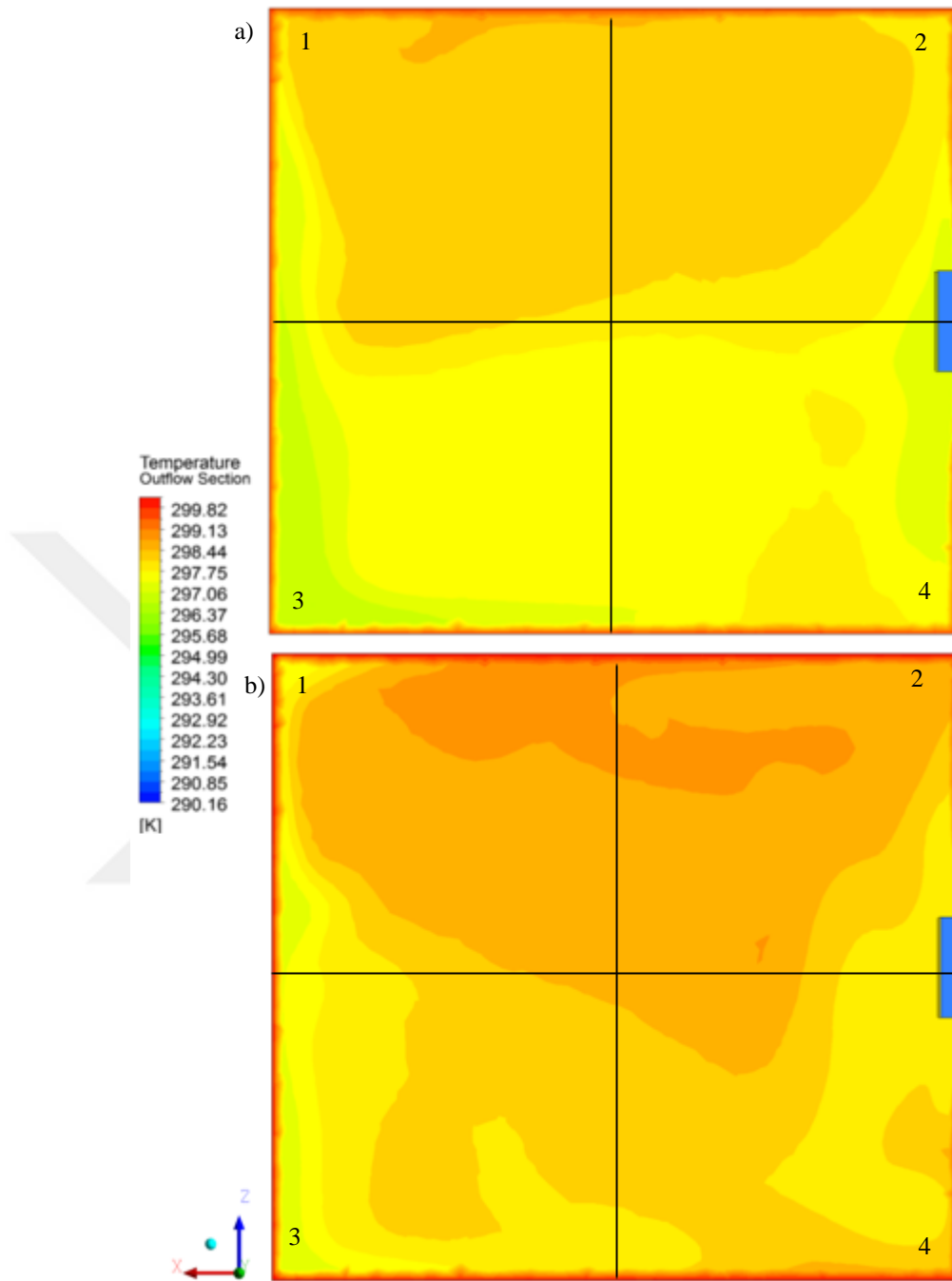


Figure 4.7 Temperature distributions at 1.70 m above ground of room: a) temperature: MIT, velocity: homogeneous, b) temperature: homogeneous, velocity: homogeneous

Table 4.2 The temperature values of the regions in Figure 4.7

Analysis	Region 1	Region 2	Region 3	Region 4
a	298.496 K	298.410 K	297.836 K	297.959 K
b	298.482 K	298.561 K	298.002 K	298.207 K

CHAPTER FIVE

CONCLUSIONS

In this study, the definition of the different boundary conditions of the outflow section of the split air conditioner indoor unit positioned in the room were investigated. The air conditioner CAD model provided by the manufacturer was used in modeling the room air volume in the CFD program. The definition of the boundary conditions, which is the main scope of the study, was carried out in the CFD program. The boundary conditions given as inputs to the outflow section of the split air conditioner indoor unit were examined with different definitions in 4 different analyses and the effects of parameters such as velocity, temperature were investigated to each other and to the flow structure.

In the numerical model, the air velocity data obtained from the Particle Image Velocimetry (PIV) system positioned at the outflow section of the air conditioner was used as the velocity input. A method which is called Meshed Infrared Thermography (MIT) method also has been developed in order to obtain temperature data of air which is transparent in the infrared wavelength with the infrared camera. The temperature data obtained using the MIT method was used as a temperature input. A new code has been developed so that the experimental data can be entered in accordance with the CFD program. By means of the code, the positions of the experimental data and the positions in the CFD program were matched and the matching data was selected and the program was entered.

In numerical analyses of conditioned air in the literature, there is no study on the use of experimental data as a boundary condition for velocity and temperature. The present study has shown that flow structure, temperature distribution and velocity distribution are influenced by boundary conditions definitions. For this reason, it is advisable to use experimental data as the boundary condition in analyses which the conditioned air in the room is investigated. Thus, while the behavior of the indoor unit of the air conditioner in the room is numerically investigated, the boundary conditions defined on the outflow section represent more realistic situations.

In addition to all these, a 3D version of the background-oriented Schlieren technique, a quantitative flow imaging method, was studied and results were obtained. The results obtained were compared with PIV, which is accepted method in the literature and the accuracy of the 3DBOS method has been proven. In cases where it is desired to quantitatively analyze flow structures, the 3DBOS method is recommended with reasonable price and ease of application.

In future work, in addition to the realistic modeling of the outflow section of the air conditioner performed in this work, numerical studies can be made by modeling the room conditions (e.g. doors, windows and furniture) properly. Thus, an air conditioner's ideal position in a room can be determined.

REFERENCES

- Anderson, R., Hassani, V., & Kirkpatrick, A. (1991). Visualizing the air flow from cold air ceiling jets. *ASHRAE Journal*, 33, 30-35.
- Awbi HB. (1989). Application of computational fluid dynamics in room ventilation. *Build Environ*, 24, 73-84.
- Blazek, J. (2001). *Computational fluid dynamics: Principles and applications*. (1st ed.). Netherlands: Elsevier Science Ltd.
- Brohus, H. (1997). *Personal exposure to contaminant sources in ventilated rooms*. Ph.D. thesis. Aalborg University, Aalborg, Denmark.
- Cao, G ., Sivukari, M., Kurnitski, J., & Ruponen, M. (2010). PIV measurement of the attached plane jet velocity field at a high turbulence intensity level in a room. *International Journal of Heat and Fluid Flow*, 31 (5), 897–908.
- Cao, G ., Sivukari, M., Kurnitski, J., Ruponen, M., & Seppänen, O. (2010). Particle image velocimetry (PIV) application in the measurement of indoor air distribution by an active chilled beam. *Building and Environment*, 45 (9), 1932–1940.
- Cehlin, M., Moshfegh, B., & Sandberg, M. (2002). Measurements of air temperatures close to a low-velocity diffuser in displacement ventilation using an infrared camera. *Energy and Buildings*, 34, 687-698.
- Chow, W. K. (1996). Application of computational fluid dynamics in building services engineering. *Building and Environment*, 31, 425-36.
- Gad-el-Hak M. (2000). *Flow control: passive, active and reactive flow management*. Cambridge: Cambridge University Press.

- Gharib, M., Kremers, D., Koochesfahani, M.M. & Kemp, M., (2002). Leonardo's vision of flow visualization. *Experiments in Fluids*, 33, 219–223.
- Herschel, W. (1800). Experiments on the refrangibility of the visible rays of the sun. *Philosophical Transactions of the Royal Society of London*, 90, 284–292.
- Incropera, F. P., & DeWitt D. P. (1996). *Fundamentals of heat and mass transfer* (4th ed.). USA: John Wiley & Sons.
- Jones, P. J., & Whittle, G. E. (1992). Computational fluid dynamics for building air flow prediction- current status and capabilities. *Build Environ*, 27 (3), 321-38.
- Karadeniz Z.H., Kumlutaş D., Özer Ö., & Kuru F. (2011). İklimlendirilen hacimlerin akış dağılımının incelenmesinde parçacık görüntülemeli hız ölçümü verilerinin sayısal oda modeline uygulanması. *İKLİM 2011 - Ulusal İklimlendirme Kongresi*, Antalya.
- Karadeniz Z.H., Kumlutaş D., Özer Ö., Kılıç İ, & Ünsalan İ. D. (2013). Ölçüm ekranlarının akışa etkilerinin parçacık görüntülemeli hız ölçümü ile incelenmesi. *19. Ulusal Isı Bilimi ve Tekniği Kongresi*, Samsun.
- Karadeniz, Z. H., Kumlutaş, D. & Özer, Ö. (2013) Experimental visualization of the flow characteristics of the outflow of a split air conditioner indoor unit by meshed infrared thermography and stereo particle image velocimetry. *Experimental Thermal and Fluid Science*, 44, 334-344.
- Meslem, A., Nastase, I., & Allard, F. (2010). Passive mixing control for innovative air diffusion terminal devices for buildings. *Building and Environment*, 45 (12), 2679–2688.
- Nero, A. V. (1988). Controlling indoor air pollution. *Scientific American*, 258 (5), 42–48.

- Nielsen, P. V. (1974). *Flow in air conditioned rooms*, Ph.D. Thesis, Aalborg Universitet, Nordborg, Denmark.
- Nielsen, P. V. (1975). Prediction of air flow and comfort in air conditioned spaces. *ASHRAE Trans*, 81 Part II.
- Nielsen, P. V. (2015). Fifty years of CFD for room air distribution. *Building and Environment*, 91, 78-90.
- Nielsen, P.V. (1973). Berechnung der Luftbewegung in einem zwangsbelüfteten Raum. *Gesundheits-Ingenieur*, 94, 299-302.
- Özer, Ö. (2011). *Experimental investigation of velocity and temperature distribution inside a split air conditioner indoor unit*. M.Sc. Thesis, Dokuz Eylül University, İzmir.
- Özer, Ö., Kumlutaş, D., Yücekaya, U. A. (2017). Üç boyutlu arka plan konumlandırılmış yoğunluk farkı (schlieren) yöntemi ile akış yapılarının incelenmesi ve parçacık görüntülemeli hız ölçümü ile doğrulanması. *13. Ulusal Tesisat Mühendisliği Kongresi*, İzmir.
- Raffel M., Willert C., Wereley S. & Kompenhans J., (2007). *Particle image velocimetry a practical guide (2nd ed.)*. New York: Springer.
- Sun, Y., & Zhang, Y. (2007). An overview of room air motion measurement: technology and application. *HVAC&R Research*, 13 (6), 929–950.
- Venkatakrishnan, L., & Meier, G. E. A. (2004). Density measurements using the background oriented schlieren technique. *Experiments in Fluids*, 37(2), 237–247.
- Wargocki, P. (1998). *Human perception, productivity and symptoms related to indoor air quality*. Ph.D. Thesis, Technical University of Denmark, Denmark.

Zhai, Z. (2006). Application of computational fluid dynamics in building design: aspects and trends. *Indoor and Built Environment*, 15, 305-13.

